ORIGINAL ARTICLES

SPONTANEOUS RAMAN SPECTROSCOPY FOR INTRACRANIAL TUMORS DIAGNOSTICS EX VIVO

Romanishkin I.D.[1], Bikmukhametova L.R.[2], Savelieva T.A.[1,3], Goryaynov S.A.[4],
Kosyrkova A.V.[4], Okhlopkov V.A.[4], Golbin D.A.[4], Poletaeva I.Yu.[4], Potapov A.A.[4],
Loschenov V.B.[1, 2, 3]
[1]Prokhorov General Physics Institute of the Russian Academy of Sciences, Moscow, Russia
[2]ООО "BIOSPEC", Moscow, Russia
[3]National Research Nuclear University MEPhI (Moscow Engineering Physics Institute), Moscow, Russia
[4]N.N. Burdenko National Medical Research Center of Neurosurgery, Moscow, Russia

Abstract

Neurosurgery of intracranial tumors, especially of glial origin, is a non-trivial task due to their infiltrative growth. In recent years, optical methods of intraoperative navigation have been actively used in neurosurgery. However, one of the most widely used approaches based on the selective accumulation of fluorescent contrast medium (5-ALA-induced protoporphyrin IX) by the tumor cannot be applied to a significant number of tumors due to its low accumulation. On the contrary, Raman spectroscopy, which allows analyzing the molecular composition of tissues while preserving all the advantages of the method of fluorescence spectroscopy, does not require the use of an exogenous dye and may become a method of choice when composing a system for intraoperative navigation or optical biopsy.

This work presents the first results of using the principal component method to classify Raman spectra of human glioblastoma with intermediate processing of spectra to minimize possible errors from the fluorescence of both endogenous fluorophores and photosensitizers used in fluorescence navigation. As a result, differences were found in the principal component space, corresponding to tissue samples with microcystic components, extensive areas of necrosis, and foci of fresh hemorrhages. It is shown that this approach can serve as the basis for constructing a system for automatic intraoperative tissue classification based on the analysis of Raman spectra.

СПЕКТРОСКОПИЯ СПОНТАННОГО КОМБИНАЦИОННОГО РАССЕЯНИЯ ДЛЯ EX VIVO ДИАГНОСТИКИ ВНУТРИЧЕРЕПНЫХ ОПУХОЛЕЙ

И.Д. Романишкин[1], Л.Р. Бикмухаметова[2], Т.А. Савельева[1,3], С.А. Горяйнов[4],
А.В. Косырькова[4], В.А. Охлопков[4], Д.А. Гольбин[4], И.Ю. Полетаева[4], А.А. Потапов[4],
В.Б. Лощенов[1, 2, 3]
[1]Институт общей физики им. А.М.Прохорова Российской академии наук, Москва, Россия
[2]ООО «БИОСПЕК», Москва, Россия
[3]Национальный исследовательский ядерный университет «МИФИ», Москва, Россия
[4]НМИЦ нейрохирургии им.ак. Н.Н.Бурденко, Москва, Россия

Резюме

Нейрохирургия внутричерепных опухолей, особенно глиального происхождения, представляет нетривиальную задачу в силу их инфильтративного роста. В последние годы в нейрохирургии активно используются оптические методы интраоперационной навигации, однако один из наиболее широко распространенных подходов, основанный на селективном накоплении опухолью флуоресцентного контрастного вещества (5-АЛК индуцированного протопорфирина IX), не может быть применен для значимой части опухолей вследствие его низкого накопления. Напротив, спектроскопия комбинационного рассеяния, позволяющая проводить анализ молекулярного состава тканей с сохранением всех достоинств метода флуоресцентной спектроскопии, не требует при этом введения экзогенного красителя и может быть вариантом выбора при построении системы интраоперационной навигации или оптической биопсии.

Romanishkin I.D., Bikmukhametova L.R., Savelieva T.A., Goryaynov S.A., Kosyrkova A.V., Okhlopkov V.A., Golbin D.A., Poletaeva I.Yu., Potapov A.A., Loschenov V.B.
Spontaneous raman spectroscopy for intracranial tumors diagnostics *ex vivo*

В настоящей работе представлены первые результаты использования метода главных компонент для классификации спектров комбинационного рассеяния глиобластомы человека с промежуточной обработкой спектров для минимизации возможных ошибок от флуоресценции как эндогенных флуорофоров, так и фотосенсибилизаторов, используемых при флуоресцентной навигации. В результате были обнаружены различия в пространстве главных компонент, соответствующие образцам тканей с микрокистозными компонентами, обширными участками некрозов, фокусами свежих кровоизлияний. Показано, что данный подход может послужить основой для построения системы автоматической интраоперационной классификации тканей на основе анализа спектров комбинационного рассеяния.

Ключевые слова: глиобластома, оптическая биопсия, спонтанное комбинационное рассеяние, метод главных компонент.

Introduction

The main problems of intracranial tumor neurosurgery are related to the complexity of tumor border demarcation due to the peculiarities of their growth. Glial tumors are known to propagate into the healthy white matter of the brain as tumor cells move along the blood vessels and nerve tracts due to the friendly microenvironment formed by the tumor-recruited immunecompetent cells. Such infiltration into healthy tissue makes radical resection impossible without creating a significant neurological deficit for the patient. In this regard, various intraoperative navigation methods have been actively used in neurosurgery in recent years, allowing for the most accurate differentiation of tumor and normal tissues, among which the optical technologies are particularly distinguished due to their efficiency and non-invasiveness. It is well known that protoporphyrin IX induced by 5-aminolevulinic acid is used for intraoperative navigation in glioblastoma surgery [1, 2]. Recently, many other methods for determining tumor borders have been investigated, including quantitative exogenous fluorescence analysis [3, 4], endogenous fluorescence lifetime imaging [5–7], optical coherence tomography (OCT) [8], hyperspectral imaging [9], and Raman scattering spectroscopy (RSS) [10, 11]. Each of these methods has its advantages, but RSS stands out among them as it allows for direct analysis of the molecular composition of the studied tissues without introducing any dyes, which leads to additional interest in this method as a diagnostic procedure which can determine tumor tissues characterized by a low level of accumulation of fluorescent markers, for example, tissues of benign glial tumors.

The first results of an RSS-based brain tumor analysis were obtained by K. Tashibu [12]. The author investigated the relative water concentration in normal and edematous brain tissues of rats by analyzing the CH and OH groups in the range of high wavenumbers. Cytotoxic and vasogenic models of brain edema in rats were also studied [13]. The works of A. Mizuno et al. [14, 15] provide the spectra of various brain tumors containing intense peaks characteristic for lipids. These early studies provided the impetus for further study of human brain tumors.

The development of fiber-optic probes [16] was the main factor that promoted the use of RSS for *in vivo* research. S. Koljenović et al. [17] examined pig brain tissue with the use of fiber-optic probes. As a result, it is shown that the analyzed Raman spectra of gray matter are dominated by bands associated with proteins, DNA, and phosphatidylcholine, while the white matter spectra are dominated by cholesterol and sphingomyelin.

Fiber-optic probes have also contributed to experimental studies of metastasis [18]. Melanoma cells were injected into the carotid artery of mice to cause brain metastasis. Serial sections were prepared from the whole mouse brain for analysis by Fourier spectroscopy and RSS methods. While metastatic melanoma cells were not detected with Fourier-infrared spectroscopy, RSS allowed for their detection with irradiation at a wavelength of 785 nm.

Ex vivo tissue studies provided essential information about the nature and composition of normal and tumor tissues. In the above study [15], the authors used RSS and Fourier spectroscopy to study various human brain tissue samples and showed that the spectra of normal but edematous, gray and white matter were similar to the spectra of normal gray and white matter in rats. It was observed that the spectra of gliomas, neurinomas, and neurocytomas are similar to those of gray matter in rats. In the study [19], 24 Raman maps were produced from unstained and unfixed sections of 20 glioblastoma tissue samples obtained from 20 patients. The necrotic tissues were found to have increased levels of cholesterol and cholesterol ester.

C. Krafft et al. [20, 21] performed brain tissue RSS for qualitative and quantitative analysis of lipid content.

Higher levels of lipids in normal tissues and higher hemoglobin content have been reported, and a lower ratio of lipids to proteins in intracranial tumors cases. Thus, RSS can be used to differentiate between normal and tumor tissues, as well as to determine the type and degree of malignancy of the tumor.

Due to the new facts about the relative content of lipids in brain tumors, Raman spectra of lipid extracts from seven human tissue samples were obtained [22]. Glioma tissues were characterized by increased water content and reduced lipid content, the results being consistent with the data obtained in the study of pig tissues.

Raman scattering (RS) was used to discover that the ratio of phosphatidylcholine to cholesterol is higher in gliomas compared to healthy tissues. The use of RSS helped differentiate brain tumors in children from normal brain tissue and distinguish similar types of tumors from each other [23].

Some works related to intraoperative *in vivo* studies of brain tumors have been published recently. As mentioned earlier, surgical resection in the case of intracranial tumors is challenging: any residual tumor cells can lead to a relapse, while healthy tissue removal can lead to cognitive impairment. Thus, early resection, as well as maintaining the functional status of patients, are crucial to achieving optimal results.

In a study involving 10 patients [24], the authors obtained real-time Raman spectra of healthy brain tissues, tumors, and necrotic tissues in vivo in real-time mode. Another study [10] shows differences in the Raman spectra between normal and tumor tissues in terms of the position of peaks of phospholipids, proteins, and nucleic acids.

The effectiveness of RSS was compared with that of MRI, which is a standard imaging method [25]. It is crucial to recognize that modern imaging technologies, including standard MRI, do not allow for the detection of distant invasive cells of glial brain tumors, since this restriction significantly reduces the effectiveness of surgical treatment of glioma. The authors of the paper demonstrate that RSS can detect invasive tumor cells far beyond the tumor detected by MRI in humans during surgery. RSS detects an invasion at a distance of ~ 3.7 cm and ~ 2.4 cm outside the borders of the MRI contrast zone.

To sum up the above, it is possible to conclude that RSS is the option of choice for intraoperative navigation in neurosurgery of intracranial tumors, especially of glial origin. RSS has a high spatial resolution, high data collection rate, and high sensitivity to changes in the molecular composition of tissues. It can detect invasive tumor cells without slowing down the neurosurgical process and complement or replace MRI-guided neuronavigation as a method for determining tumor boundaries.

Materials and methods

A spectroscopic system consisting of a Raman-HR-TEC-785 Raman scattering spectrometer (StellarNet, USA), a narrow-band laser radiation source with a wavelength of 785 nm (the width at half the amplitude of the laser peak of 0.2 nm, power up to 500 mW) Ramulaser™ 785 (StellarNet, USA), and a fiber-optic confocal probe for laser radiation and Raman scattering signal delivery (fig. 1) was used in this study. The use of the probe made it possible to receive a signal from an area less than 0.5 mm in diameter on the sample surface. The spectrometer was controlled from a computer with the software developed by us that allows recording a series of Raman spectra. This system allows recording spectra in the range of 800–1000 nm, which corresponds to the range of Stokes shifts of 200–2750 cm^{-1}. The spectral resolution of the system was 4 cm^{-1}.

The studied material was obtained during the removal of human intracranial tumors (4 patients diagnosed with glioblastoma multiforme) and provided by the N.N. Burdenko National Medical Research Center of Neurosurgery. The material was examined under two conditions: in the operating room immediately after removal, *ex vivo* (2 patients, 7 tissue samples), and in the biobank 2 hours after removal (3 patients, 6 samples). During its transfer from the operating room to the biobank, the material was stored in saline.

The Raman spectra of each sample were recorded in a series of 5 measurements, with subsequent averaging. The exposure time of each measurement was 30 seconds (a total of 2.5 minutes per series) due to the technical limitations of the spectrometer used. Before each series, the background was measured (a series of 5 spectra of 30 seconds each), with the laser turned off. The background signal and Raman spectrum were measured in a darkened room.

During preprocessing, the spectra were first averaged within each series to reduce the contribution of random noise to the resulting signal. The corresponding average background spectrum was then subtracted from the average Raman spectra to exclude errors caused by the measurement conditions.

The obtained spectra were characterized by a high intensity of fluorescence, which is a noise signal for the RSS and worsens its decoding properties. To exclude the fluorescence component from the recorded signal, the algorithm presented in the paper [26] was used (Fig. 2). The method uses a continuous wavelet transform to determine the position of sharp Raman peaks and subtract the smooth background signal. The resulting spectrum was smoothed by a third-order Savitzky–Golay filter.

One of the difficulties in characterizing a tissue sample from the Raman spectrum is due to the high dimensionality of the obtained spectra, i.e., a large number of significant Raman peaks from various organic compounds.
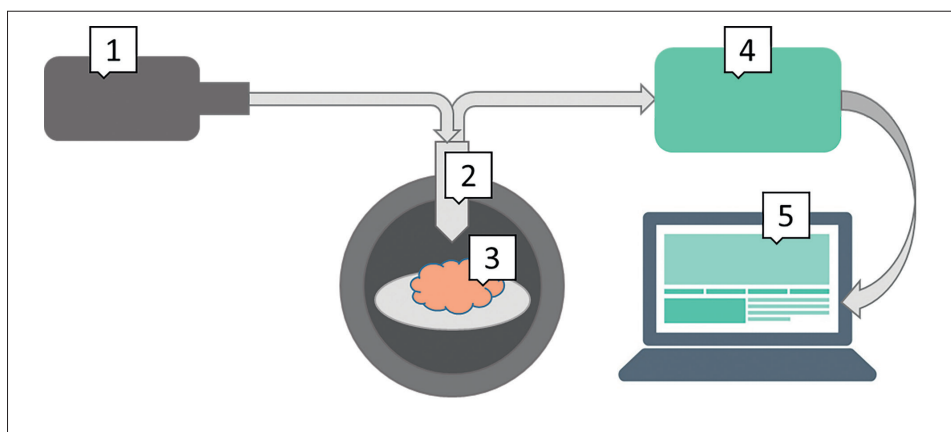
Romanishkin I.D., Bikmukhametova L.R., Savelieva T.A., Goryaynov S.A., Kosyrkova A.V.,
Okhlopkov V.A., Golbin D.A., Poletaeva I.Yu., Potapov A.A., Loschenov V.B.
Spontaneous raman spectroscopy for intracranial tumors diagnostics *ex vivo*

Рис. 1. Схема рабочей установки:
1. Источник узкополосного лазерного излучения с длиной волны 785 нм
2. Волоконно-оптический конфокальный зонд для доставки лазерного излучения и сигнала КР
3. Исследуемый образец биологической ткани
4. Спектрометр комбинационного рассеяния света
5. Компьютер со специальным программным обеспечением

Fig. 1. Working setup diagram:
1. Source of 785 nm narrow-band laser radiation
2. Fiber optic confocal probe for delivery of laser radiation and Raman signal
3. Sample of biological tissue
4. Raman spectrometer
5. Computer with special software

Raman spectra, unlike, for example, fluorescence spectra, are characterized by a large number of characteristic spectral lines, and their visual interpretation becomes a non-trivial task. To solve this problem, the principal component analysis (PCA) method was used as a dimensionality reduction method. Each spectrum represents a point on a hyperplane with a dimension corresponding to the number of values in the measured Raman spectrum. The PCA method rotates the coordinate system so that the axes lie along the data in the direction of the largest dispersion. With this rotation, each principal component is a linear combination of values along the original axes. At the same time, we do not need to consider those axes on which the data spread after such a rotation is minimal. This provides dimensionality reduction.

Results and discussion

Raman spectra of human glioma tissue specimens were obtained. Each of the samples was verified as glioblastoma multiforme WHO Grade IV. Foci of necrosis and vascular proliferation were found in all samples.

The Raman spectra obtained from each of the samples were processed according to the above methods. This allowed us to obtain spectra with minimized measurement errors and free from the fluorescent signal. As an example, fig. 3 shows the Raman spectra for patient K with the selection of the main peaks that characterize biomolecules whose content is increased in tumor tissues.

Patient K had the following distribution of material by biopsy: 1 – tumor, 20% necrosis; 2 – tumor, less than 30% necrosis; 3 – tumor, less than 40% necrosis, pronounced angiomatosis; 4 – tumor, up to 90% necrosis (of vascular genesis, being a conglomerate of thick-walled vessels and adjacent tumor tissue). The difference in the composition of the material is manifested in the difference in the intensity of the Raman peaks; however, the peaks that characterize glial tumors remain clearly visible (Fig. 3). Fig. 3 shows the significant contribution of cholesterol, protein, disaccharide, and nitrogenous bases into the process. As shown in the works of [19, 22], cholesterol can be associated with necrosis, which corresponds to the data of tumor specimen morphological studies.

The main components were analyzed in the spectral range of 900–1700 cm^{-1}, since it is in this region that the peaks characteristic of glial tumors predominate [27]. The main spectral features were observed for protein (1236, 1239 cm^{-1}), nitrogenous bases (1181, 1572 cm^{-1}), disaccharide (1461 cm^{-1}), deoxyribose (1430 cm^{-1}), and cholesterol (1085, 1296, 1032, 1451, 1659 cm^{-1}), acyl residues of lipids (1086 cm^{-1}) and phospholipids (1129 cm^{-1}).

The PCA result showed that the main differences (71% of the variance) are explained by the first two principal components (Fig. 4). If we consider the load spectra (how strongly the Raman signal affects the value of the principal component) of the first two components (Fig. 5), we can see a positive contribution of the Raman signal in the range of 1300–1450 cm^{-1} to the value of PC1,
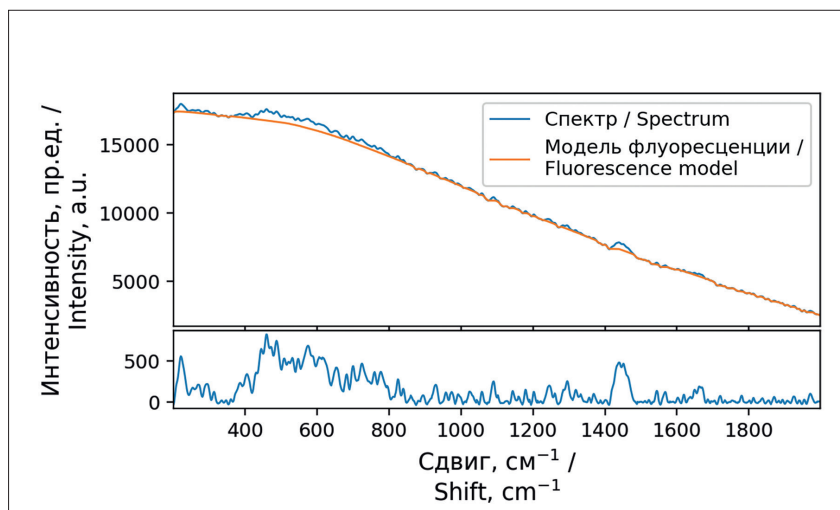
Рис. 2. Работа метода вычитания флуоресцентного сигнала из спектра КР. Сверху – измеренный спектр КР и построенная методом [26] модель гладкого спектра флуоресценции. Снизу – спектр КР без флуоресценции
Fig. 2. The work of the method of subtracting the fluorescent signal from the Raman spectrum. Above are the measured Raman spectrum and the smooth fluorescence spectrum model constructed by the method [26]. Below is the Raman spectrum without fluorescence
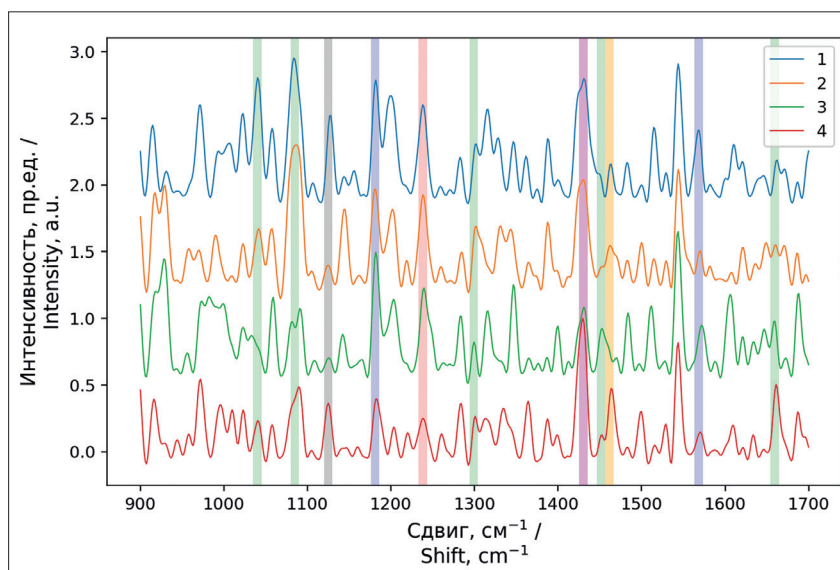

Рис. 3. Спектры КР образцов ткани пациента К. Значения интенсивности нормированы на максимум и смещены для удобства представления. Вертикальными полосами обозначены пики, характеризующие биомолекулы, содержание которых повышено в опухолевых тканях: белки (1236, 1239 см⁻¹, красный), азотистые основания (1181, 1572 см⁻¹, синий), дисахарид (1461 см⁻¹, желтый), дезоксирибоза (1430 см⁻¹, пурпурный), фосфолипид (1129 см⁻¹, серый), холестерин (1085, 1296, 1032, 1451, 1659 см⁻¹, зеленый)
Fig. 3. Raman spectra of patient K. tissue samples. Intensity values are normalized to a maximum and shifted for ease of presentation. The vertical lines indicate the peaks characterizing the biomolecules, the content of which is higher in tumor tissues: proteins (1236, 1239 cm⁻¹, red), nitrogenous bases (1181, 1572 cm⁻¹, blue), disaccharide (1461 cm⁻¹, yellow), deoxyribose (1430 cm⁻¹, magenta), and phospholipid (1129 cm⁻¹, gray), cholesterol (1085, 1296, 1032, 1451, 1659 cm⁻¹, green)
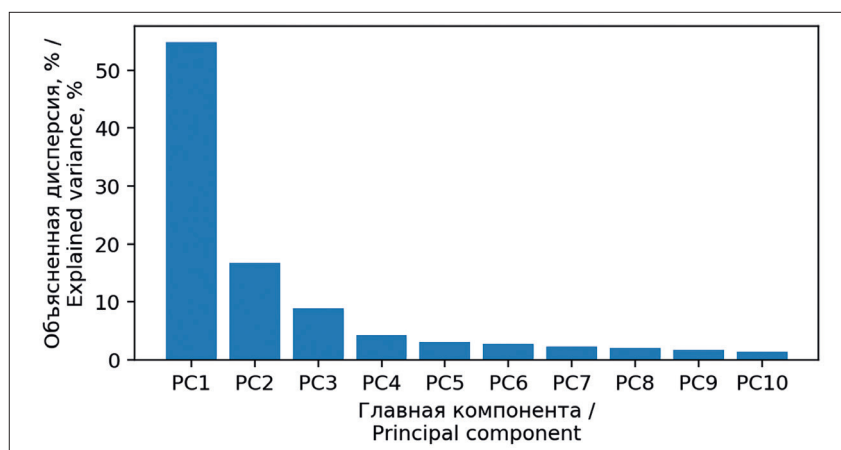
Рис. 4. Собственные значения главных компонент
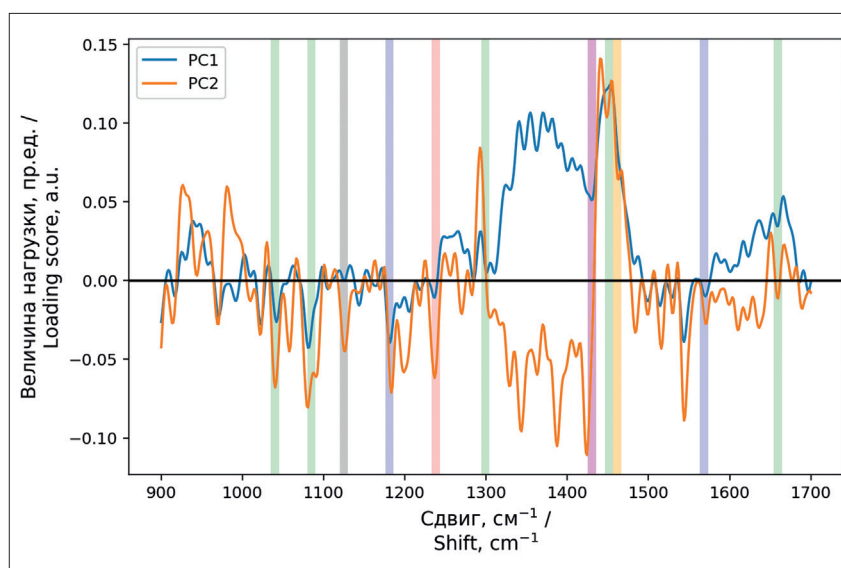**Fig. 4.** Eigenvalues of the principal components

Рис. 5. Спектры нагрузки для первых двух главных компонент. Цветом выделены сдвиги, соответствующие биомолекулам, содержание которых повышено в опухолевых тканях (см. рис. 3)
Fig. 5. Loading score spectra for the first two principal components. Highlighted in color are the shifts corresponding to biomolecules, the content of which is higher in tumor tissues (see Fig. 3)

probably caused by high blood content. In this case, the PC2 value decreases with the increase of the signal from proteins, nitrogenous bases, and cholesterol (values at shifts of 1032 and 1085 cm^{-1}).

Distributions of the measured spectra from the first two principal components were obtained (Fig. 5, left). The material measured in the operating room forms a dense group in the third quarter of the PC1/PC2 coordinate plane. At the same time, no groups of measured samples are formed on the PC1/PC3 plane (Fig. 5, on the right), which suggests that the use of more than two main components when considering the

measured data set is redundant. The Raman spectra of specimens from patient B, characterized by a massive hemorrhage, also lie in the negative PC1 range. The pathomorphological description of the tumor tissues of patient B showing the highest differences from the rest of the analysis by principal component method includes, in addition to the basic features of glioblastoma, such features as gliomezodermal scar tissue, and the presence of microcystic component, large areas of necrosis, and foci of fresh hemorrhage in the tumor. The pattern corresponds to glioblastoma with therapeutically induced changes.
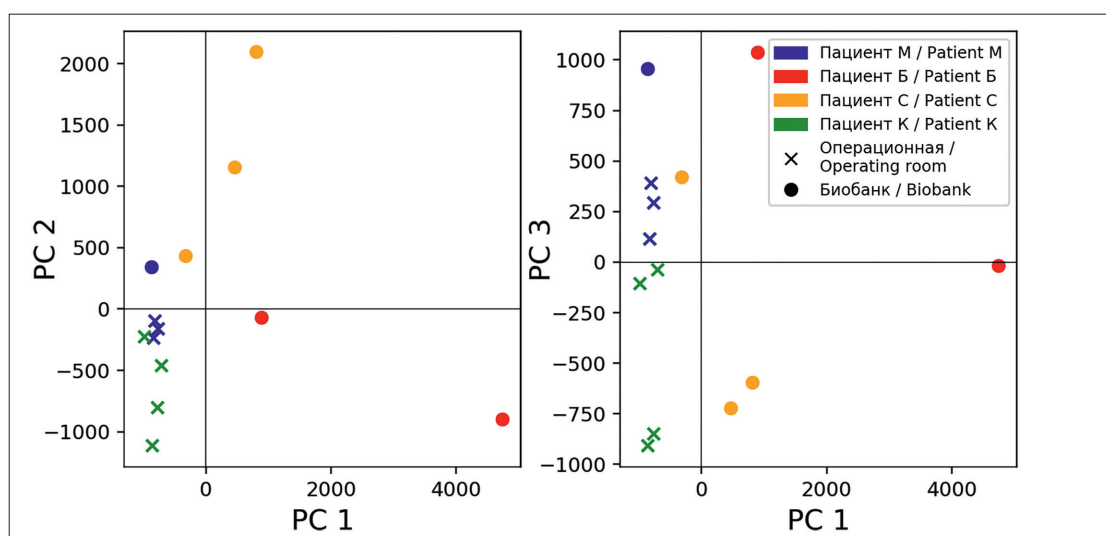
Рис. 6. Анализ главных компонент спектров КР образцов опухолевой ткани четырех пациентов, измеренных в операционной ex vivo и в биобанке
Fig. 6. PCA of the Raman spectra of tumor tissue samples from four patients, measured in the operating room ex vivo and in the biobank

The pathomorphological description of patient C's tissues also mentioned, against the background of the main features of multiform glioblastoma, microcystic structure, and foci of recent hemorrhages.

Conclusion

The paper presents the first results of the main component method for classification of spectra of glioblastoma tissue samples with intermediate processing of spectra to minimize possible errors due to fluorescence of both endogenous fluorophores and photosensitizers used in fluorescent navigation. There are differences in the principal components corresponding to tissue samples with microcystic components, extensive areas of necrosis, and foci of recent hemorrhages. A further set of data from different types of brain pathologies will enable clustering and analysis of the spectra [28] to build an intraoperative diagnostic system based on automatic Raman spectra analysis.

REFERENCES

1. Stummer W., Pichlmeier U., Meinel T., Wiestler O.D., Zanella F., Reulen H.J. Fluorescence-guided surgery with 5-aminolevulinic acid for resection of malignant glioma: a randomised controlled multicentre phase III trial, *Lancet Oncol*, 2006, vol. 7 (5), pp. 392–401.
2. Potapov A.A., Goriaïnov S.A., Loshchenov V.B., Savel'eva T.A., Gavrilov A.G., Okhlopkov V.A. Intraoperative combined spectroscopy (optical biopsy) of cerebral gliomas, *Zh. Vopr. Neirokhir. Im. N.N. Burdenko*, 2013, vol. 77 (2), pp. 3–10.
3. Valdes P.A., Jacobs V.L., Wilson B.C., Leblond F., Roberts D.W., Paulsen K.D. System and methods for wide-field quantitative fluorescence imaging during neurosurgery, *Opt. Lett.*, 2013, vol. 38 (15), pp. 2786.
4. Savelieva T.A., Loshchenov M.V., Borodkin A.V., Linkov K.G., Kosyrkova A.V., Goryajnov S.A., et al. Combined spectroscopic and video fluorescent instrument for intraoperative navigation when removing a glial tumor, *SPIE Photonics Europe*, 2020, vol. 11363. doi: 10.1117/12.2556064
5. Marcu L., Jo J.A., Butte P.V., Yong W.H., Pikul B.K., Black K.L., Thompson R.C. Fluorescence Lifetime Spectroscopy of Glioblastoma Multiforme, *Photochem. Photobiol.*, 2004., vol. 80 (1), pp. 98.

ЛИТЕРАТУРА

1. Stummer W., Pichlmeier U., Meinel T. et al. Fluorescence-guided surgery with 5-aminolevulinic acid for resection of malignant glioma: a randomised controlled multicentre phase III trial // Lancet Oncol. – 2006. – Vol. 7(5). – P. 392–401.
2. Potapov A.A., Goriaïnov S.A., Loshchenov V.B. Intraoperative combined spectroscopy (optical biopsy) of cerebral gliomas // Zh. Vopr. Neirokhir. Im. N.N. Burdenko. – 2013. – Vol. 77(2). – P. 3–10.
3. Valdes P.A., Jacobs V.L., Wilson B.C. et al. System and methods for wide-field quantitative fluorescence imaging during neurosurgery // Opt. Lett. – 2013. – Vol. 38(15). – P. 2786.
4. Savelieva T.A., Loshchenov M.V., Borodkin A.V. et al. Combined spectroscopic and video fluorescent instrument for intraoperative navigation when removing a glial tumor // SPIE Photonics Europe. – 2020. – Vol. 11363. DOI: 10.1117/12.2556064
5. Marcu L., Jo J.A., Butte P.V. et al. Fluorescence Lifetime Spectroscopy of Glioblastoma Multiforme // Photochem. Photobiol. – 2004. – Vol. 80(1). – P. 98.
6. Butte P.V., Mamelak A.N., Nuno M. et al. Fluorescence lifetime spectroscopy for guided therapy of brain tumors // Neuroimage. – 2011. – Vol. 54, Suppl. 1. – S125-S135.

6. Butte P.V., Mamelak A.N., Nuno M., Bannykh S.I., Black K.L., Marcu L. Fluorescence lifetime spectroscopy for guided therapy of brain tumors, *Neuroimage*, 2011, vol. 54, suppl. 1, s125–s135.

7. Kantelhardt S.R., Kalasauskas D., König K., Kim E., Weinigel M., Uchugonova A., Giese A. In vivo multiphoton tomography and fluorescence lifetime imaging of human brain tumor tissue, *J. Neurooncol.*, 2016., vol. 127 (3), pp. 473–482.

8. Kut C., Chaichana K.L., Xi J., Raza S.M., Ye X., McVeigh E.R., Rodriguez F.J. Detection of human brain cancer infiltration ex vivo and in vivo using quantitative optical coherence tomography, *Sci. Transl. Med.*, 2015, vol. 7 (292), 292ra100–292ra100.

9. Fabelo H., Ortega S., Lazcano R., Madroñal D., Callicó G.M., Juárez E. An Intraoperative Visualization System Using Hyperspectral Imaging to Aid in Brain Tumor Delineation, *Sensors*, 2018, vol. 18 (2), pp. 430.

10. Jermyn M., Mok K., Mercier J., Desroches J., Pichette J., Saint-Arnaud K., Intraoperative brain cancer detection with Raman spectroscopy in humans, *Sci. Transl. Med.*, 2015, vol. 7 (274), 274ra19–274ra19.

11. Brusatori M., Auner G., Noh T., Scarpace L., Broadbent B., Kalkanis S.N. Intraoperative Raman Spectroscopy, *Neurosurg. Clin. N. Am.*, 2017, vol. 28 (4), pp. 633–652.

12. Tashibu K. Analysis of water content in rat brain using Raman spectroscopy, No To Shinkei, 1990, vol. 42 (10), pp. 999–1004.

13. Kitajima T., Tashibu K., Tani S., Mizuno A., Nakamura N. Analysis of water content in young rats brain edema by Raman spectroscopy, *No To Shinkei*, 1993, vol. 45 (6), pp. 519–524. [in Japan.]

14. Mizuno A., Hayashi T., Tashibu K., Maraishi S., Kawauchi K., Ozaki Y. Near-infrared FT-Raman spectra of the rat brain tissues, *Neurosci. Lett.*, 1992, vol. 141 (1), pp. 47–52.

15. Mizuno A., Kitajima H., Kawauchi K., Muraishi S., Ozaki Y. Near-infrared Fourier transform Raman spectroscopic study of human brain tissues and tumours, *J. Raman Spectrosc.*, 1994, vol. 25 (1), pp. 25–29.

16. Beleites C., Geiger K., Kirsch M., Sobottka S.B., Schackert G., Salzer R. Raman spectroscopic grading of astrocytoma tissues: Using soft reference information, *Anal. Bioanal. Chem.*, 2011, vol. 400 (9), pp. 2801–2816.

17. Koljenović S., Schut T.C., Wolthuis R., Vincent A.J., Hendriks-Hagevi G., Santos L., et al. Raman spectroscopic characterization of porcine brain tissue using a single fiber-optic probe, *Anal. Chem.*, 2007, vol. 79 (2), pp. 557–564.

18. Krafft C., Kirsch M., Beleites C., Schackert G., Salzer R. Methodology for fiber-optic Raman mapping and FTIR imaging of metastases in mouse brains, *Anal. Bioanal. Chem.*, 2007, vol. 389 (4), pp. 1133–1142.

19. Koljenović S., Choo-Smith L.-P., Schut T.C.B., Kros J.M., van den Berge H.J., Puppels G.J. Discriminating vital tumor from necrotic tissue in human glioblastoma tissue samples by Raman spectroscopy, *Lab. Investig.*, 2002, vol. 82 (10), pp. 1265–1277.

20. Krafft C., Neudert L., Simat T., Salzer R. Near infrared Raman spectra of human brain lipids, *Spectrochim. Acta – Part A Mol. Biomol. Spectrosc.*, 2005, vol. 61 (7), pp. 1529–1535.

21. Krafft C., Sobottka S.B., Schackert G., Salzer R. Near infrared Raman spectroscopic mapping of native brain tissue and intracranial tumors, *Analyst*, 2005, vol. 130 (7), pp. 1070–1077.

22. Köhler M., Machill S., Salzer R., Krafft C. Characterization of lipid extracts from brain tissue and tumors using Raman spectroscopy and mass spectrometry, *Anal. Bioanal. Chem.*, 2009, vol. 393 (5), pp. 1513–1520.

23. Leslie D.G., Kast R.E., Poulik J.M., Rabah R., Sood S., Auner G.W., et al. Identification of pediatric brain neoplasms using raman spectroscopy, *Pediatr. Neurosurg.*, 2012. vol. 48 (2), pp. 109–117.

24. Desroches J., Jermyn M., Mok K., Lemieux-Leduc C., Mercier J., St-Arnaud K. et al. Characterization of a Raman spectroscopy probe system for intraoperative brain tissue classification, *Biomed. Opt. Express*, 2015, vol. 6 (7), pp. 2380.

7. Kantelhardt S.R. Kalasauskas D., König K., et al. In vivo multiphoton tomography and fluorescence lifetime imaging of human brain tumor tissue // J. Neurooncol. – 2016. – Vol. 127(3). – P. 473–482.

8. Kut C., Chaichana K.L., Xi J., et al. Detection of human brain cancer infiltration ex vivo and in vivo using quantitative optical coherence tomography // Sci. Transl. Med. – 2015. Vol. 7(292). – 292ra100.

9. Fabelo H., Ortega S., Lazcano R., et al. An Intraoperative Visualization System Using Hyperspectral Imaging to Aid in Brain Tumor Delineation // Sensors. – 2018. – Vol. 18(2). – P. 430.

10. Jermyn M., Mok K., Mercier J. Intraoperative brain cancer detection with Raman spectroscopy in humans // Sci. Transl. Med. – 2015. – Vol. 7(274). – 274ra19.

11. Brusatori M., Auner G., Noh T., et al. Intraoperative Raman Spectroscopy // Neurosurg. Clin. N. Am. – 2017. – Vol. 28(4). – P. 633–652.

12. Tashibu K. Analysis of water content in rat brain using Raman spectroscopy // No To Shinkei. – 1990. – Vol. 42(10). – P. 999–1004.

13. Kitajima T., Tashibu K., Tani S., et al. Analysis of water content in young rats brain edema by Raman spectroscopy // No To Shinkei. – 1993. – Vol. 45(6). – P. 519–524.

14. Mizuno A., Hayashi T., Tashibu K., et al. Near-infrared FT-Raman spectra of the rat brain tissues // Neurosci. Lett. – 1992. – Vol. 141(1). – P. 47–52.

15. Mizuno A., Kitajima H., Kawauchi K., et al. Near-infrared Fourier transform Raman spectroscopic study of human brain tissues and tumours // J. Raman Spectrosc. – 1994. Vol. 25(1). – P. 25–29.

16. Beleites C., Geiger K., Kirsch M., et al. Raman spectroscopic grading of astrocytoma tissues: Using soft reference information // Anal. Bioanal. Chem. – 2011. – Vol. 400(9). – P. 2801–2816.

17. Koljenović S., Schut T.C., Wolthuis R., et al. Raman spectroscopic characterization of porcine brain tissue using a single fiber-optic probe // Anal. Chem. – 2007. – Vol. 79(2). – P. 557–564.

18. Krafft C., Kirsch M., Beleites C., et al. Methodology for fiber-optic Raman mapping and FTIR imaging of metastases in mouse brains // Anal. Bioanal. Chem. – 2007. – Vol. 389(4). – P. 1133–1142.

19. Koljenović S., Choo-Smith L.-P., Schut T.C.B., et al. Discriminating vital tumor from necrotic tissue in human glioblastoma tissue samples by Raman spectroscopy // Lab. Investig. – 2002. – Vol. 82(10). – P. 1265–1277.

20. Krafft C., Neudert L., Simat T., et al. Near infrared Raman spectra of human brain lipids // Spectrochim. Acta - Part A Mol. Biomol. Spectrosc. – 2005. – Vol. 61(7). – P. 1529–1535.

21. Krafft C., Sobottka S.B., Schackert G. et al. Near infrared Raman spectroscopic mapping of native brain tissue and intracranial tumors // Analyst. – 2005. – Vol. 130(7). – P. 1070–1077.

22. Köhler M., Machill S., Salzer R., et al. Characterization of lipid extracts from brain tissue and tumors using Raman spectroscopy and mass spectrometry // Anal. Bioanal. Chem. – 2009. – Vol. 393(5). – P. 1513–1520.

23. Leslie D.G., Kast R.E., Poulik J.M., et al. Identification of pediatric brain neoplasms using raman spectroscopy // Pediatr. Neurosurg. – 2012. – Vol. 48(2). – P. 109–117.

24. Desroches J., Jermyn M., Mok K., et al. Characterization of a Raman spectroscopy probe system for intraoperative brain tissue classification // Biomed. Opt. Express. – 2015. – Vol. 6(7). – P. 2380.

25. Jermyn M., Desroches J., Mercier J., et al. Raman spectroscopy detects distant invasive brain cancer cells centimeters beyond MRI capability in humans // Biomed. Opt. Express. – 2016. – Vol. 7(12). – P. 5129.

26. Zhang Z.-M., Chen S., Liang Y.-Z., et al. An intelligent background-correction algorithm for highly fluorescent samples in Raman spectroscopy // J. Raman Spectrosc. – 2009. – Vol. 41(6). – P. 659–669.

25. Jermyn M., Desroches J., Mercier J., St-Arnaud K., Guiot M.-C., Leblond F., et al. Raman spectroscopy detects distant invasive brain cancer cells centimeters beyond MRI capability in humans, *Biomed. Opt. Express*, 2016, vol. 7 (12), pp. 5129.

26. Zhang Z.-M., Chen S., Liang Y.-Z., Liu Z.-X., Zhang Q.-M., Ding L.-X., et al. An intelligent background-correction algorithm for highly fluorescent samples in Raman spectroscopy, *J. Raman Spectrosc.*, 2009, vol. 41 (6), pp. 659–669.

27. Bikmukhametova L. R., Romanishkin I. A., Savelieva T. A., Skobeltsin A. S., Maklygina Yu. S., Loschenov V.B., et al. Spontaneous Raman Spectroscopy for Intracranial Tumor Diagnostics, *J. Phys. Conf. Ser.*, 2020, vol. 1439 (1), 012038.

28. Osmakov I. A., Savelieva T. A., Loschenov V. B., Goryajnov S. A., Potapov A. A. Cluster analysis of the results of intraoperative optical spectroscopic diagnostics in brain glioma neurosurgery, *Biomed. Photonics*, 2018, vol. 7 (4), pp. 23–34.

27. Bikmukhametova L.R., Romanishkin I.A., Savelieva T.A. et al. Spontaneous Raman Spectroscopy for Intracranial Tumor Diagnostics // J. Phys. Conf. Ser. – 2020. – Vol. 1439(1). – P. 012038.

28. Osmakov I.A., Savelieva T.A., Loschenov V.B., et al. Cluster analysis of the results of intraoperative optical spectroscopic diagnostics in brain glioma neurosurgery // Biomed. Photonics. – 2018. – Vol. 7(4). – P. 23–34.

ORIGINAL ARTICLES

BMP

POSSIBILITIES OF PAIN MANAGEMENT DURING PHOTODYNAMIC THERAPY

Shinkarev S.A.[1, 2], Borisov V.A.[1, 2], Boldyrev S.V.[1],
Podolsky V.N.[1], Abdurashidov Z.I.[1], Zagadaev A.P.[1, 2], Klycheva O.N.[1]
[1]Lipetsk State Oncology Clinic, Lipetsk, Russia
[2]Voronezh State Medical University named after N.N. Burdenko, Voronezh, Russia

Abstract

The authors consider the possibilities of pain management during photodynamic therapy (PDT) of visible tumors based on the observation of 102 patients. Of the total number of patients, 62 had verified basal cell skin cancer, 10 people - squamous cell skin cancer, another 10 - oral and oropharynx mucosa cancer, 8 – oral leukoplakia and dysplasia, in 6 - lower lip cancer, in 4 - breast cancer, in 2 - other localizations of neoplasms. In 15 patients, nonsteroidal anti-inflammatory drugs (NSAID) were used as pain management, in 69 - a combination of NSAID with tramadol, in 14 - nerve block anesthesia, in 4 - PDT was performed under general anesthesia.
The intensity of pain syndrome during laser irradiation of the tumor was assessed on the verbal rating scale (VRS). The absence of pain was recorded in 9% of cases. Mild pain was noted by 58% of patients, moderate pain - 20%, severe pain - 10%, very severe pain was noted by 3% of patients. The degree of expression of pain syndrome during PDT depends on the incidence of a lesion, histological form of tumor, and method of anesthesia. NSAID alone, or in combination with an opioid analgesic, allows effective control of pain syndrome in PDT of basal cell skin cancer in 89%, in PDT of squamous cell skin cancer in 66% of observations. Nerve block anesthesia allows stoping pain syndrome during PDT of oropharyngeal tumors.

ВОЗМОЖНОСТИ ОБЕЗБОЛИВАНИЯ ПРИ ФОТОДИНАМИЧЕСКОЙ ТЕРАПИИ

С.А. Шинкарев[1, 2], В.А. Борисов[1, 2], С.В. Болдырев[1],
В.Н. Подольский[1], З.И. Абдурашидов[1], А.П. Загадаев[1, 2], О.Н. Клычева[1]
[1]Липецкий областной онкологический диспансер, Липецк, Россия
[2]Воронежский государственный медицинский университет им. Н.Н. Бурденко, Воронеж, Россия

Резюме

Авторы рассматривают возможности обезболивания при фотодинамической терапии (ФДТ) опухолей визуальных локализаций на основе анализа данных 102 пациентов. Среди пациентов, включенных в выборку, у 62 верифицирован базальноклеточный рак кожи, у 10 – плоскоклеточный рак кожи, у 10 – рак слизистой оболочки полости рта и ротоглотки, у 8 – лейкоплакия и дисплазия слизистой оболочки полости рта, у 6 – рак нижней губы, у 4 – рак молочной железы, у 2 – новообразования иных локализаций.
У 15 пациентов для обезболивания применяли нестероидные противовоспалительные препараты (НПВС), у 69 – сочетание НПВС со слабыми опиоидами (трамадолом), у 14 – проводниковую анестезию, у 4 ФДТ проводили под общим обезболиванием.
Интенсивность болевого синдрома оценивалась в процессе проведения лазерного облучения опухоли по шкале вербальных оценок (ШВО). Отсутствие болевых ощущений зафиксировано в 9% наблюдений. Слабую боль отмечали в 58% наблюдений, умеренную боль – в 20%, сильную боль – в 10%, очень сильную боль – в 3% наблюдений.
Степень выраженности болевого синдрома при проведении ФДТ зависит от распространенности поражения, гистологической формы опухоли и способа обезболивания. НПВС в самостоятельном варианте или в сочетании с опиоидным анальгетиком позволяют эффективно контролировать болевой синдром при ФДТ базальноклеточного рака кожи в 89%, плоскоклеточного рака кожи – в 66% наблюдений. Проводниковая анестезия позволяет купировать болевой синдром при проведении ФДТ опухолей орофарингеальной области.

Introduction

Photodynamic therapy (PT) is a dynamically developing modern method of treatment of malignant neoplasms and a number of pre-tumor diseases and conditions (leukoplakia and dysplasia of the oral mucousa, actinic skin keratosis, vulva kraurosis, etc.) [1]. One of the important practical aspects of the use of tumor PDT in clinical practice is the problem of pain relief. It is not recommended to use local infiltration anesthesia for pain relief during PDT, which is why the most commonly used non-steroidal anti-inflammatory drugs (NSAIDs), opioid analgesics (tramadol, promedol), sedative medications (Phenosepam, Diphenhydramine, Relanium), are administered parenterally 40–60 minutes before the procedure. When tumors are localized on the skin and mucous membranes, local anesthetics can be used in the form of an ointment (applied on the skin) or by irrigation of the mucous membrane with lidocaine solution [2]. In some cases, PDT is performed with spinal anesthesia or with general anesthesia; cooled air and conduction anesthesia are also used [3].

The intensity of the pain syndrome grows with increasing laser power density and with a large area of exposure [4, 5]. In addition, for a number of photosensitizers such as derivatives of phthalocyanine, M-tetrahydroxophenyl chloride (mTHPC), laser irradiation resulted in a high degree of pain [6]. Insufficient level of analgesia may result in patients' refusal to continue treatment [7].

A significant proportion of patients receiving PDT are elderly and senile. These patients usually have multiple comorbidities that limit the use of NSAIDs and opioid analgesics. Older people are often not prepared to tolerate the minor pain associated with PDT. With tumor localization on the mucous membrane of the oral cavity, oropharynx, lower lip, or genitals, photodynamic reaction causes a high intensity pain.

Materials and methods

Our study included 102 patients treated with PDT. The treatment was performed at the Lipetsk Regional Cancer Center from January 2017 to September 2019. Photosensitizers of the chlorin series were used: Radachlorin (LLC "Rada-PHARMA", Russia, registration certificate No. LS-001868 from 16.12.2011) at a dose of 1.0–1.2 mg/kg of body weight, Photolon (RUE Belmedpreparaty, Republic of Belarus, registration certificate П N015948/01 of No-

vember 30, 2012) at the rate of 2.0–2.5 mg/kg of body weight, photoran e6 (OOO "Kompaniya DEKO", Russia, registration certificate No. LP-004885, dated 13.06.2018) at a dose of 2.0–2.5 mg/kg of body weight. The calculated dose of the drug was dissolved in 200 ml of 0.9% sodium chloride solution administered IVFD for 30 minutes. Photosensitizer exposure time was 3 hours. Irradiation was performed with MILON-LAKHTA laser (OOO "Milon Laser", Russia) with a wavelength of 662 nm. The tumors were irradiated with macro- and microlenses.

The study included 102 patients, 62 of them with verified basal cell skin cancer, 10 with squamous cell skin cancer, 10 with cancer of the oral mucosa and oropharynx, 8 with leukoplakia and dysplasia of the oral mucosa, 6 with lower lip cancer, 4 with intradermal metastases of breast cancer, 2 with other localization of the pathological process. In 40% of cases, PDT was performed for recurrent neoplasms. 69% of patients were 70 years old or older at the time of treatment.

The average diameter of the pathological focus was 34 ± 27.8 mm, and the average number of foci per patient was 1.3. In 55% of cases, the diagnosis was verified cytologically, and in 45% histologically. The average number of radiation fields per patient was 2.7, and the average diameter of the radiation field was 27 ± 12.5 mm. The power density of the laser radiation was 469 ± 261 mW/cm^2, and the dose density per field was 258 ± 99.7 J/cm^2.

The intensity of the pain syndrome was assessed during laser irradiation of the tumor on a verbal rating scale (VRS): 0 – no pain, 1 point – mild, 2 – moderate, 3 – severe, 4 – very severe or unbearable pain (Fig. 1) [8].

Results and discussion

When performing laser irradiation of the tumor during PDT against the background of using one or another method of anesthesia, the absence of pain was recorded in 9% of cases, mild pain was stated by the majority of patients, 58%, moderate pain by 20%, severe pain by 10%, very severe pain by 3% of patients (Fig. 2).

15 patients were administered NSAIDs for analgesia, 69 had a combination of NSAIDs with tramadol, 14 had conduction anesthesia? and 4 had PDT under general anesthesia. Analgesia options in PDT depending on the localization and histological form of the tumor are shown in Fig. 3.

The analyzis of factors that affect the intensity of pain revealed that the least pronounced pain syndrome
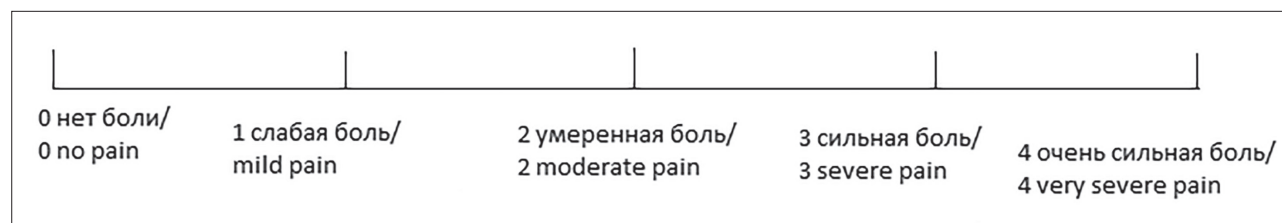
Shinkarev S.A., Borisov V.A., Boldyrev S.V., Podolsky V.N., Abdurashidov Z.I., Zagadaev A.P., Klycheva O.N.
Possibilities of pain management during photodynamic therapy

BMP

ORIGINAL ARTICLES

Рис. 1. Шкала вербальных оценок интенсивности болевого синдрома
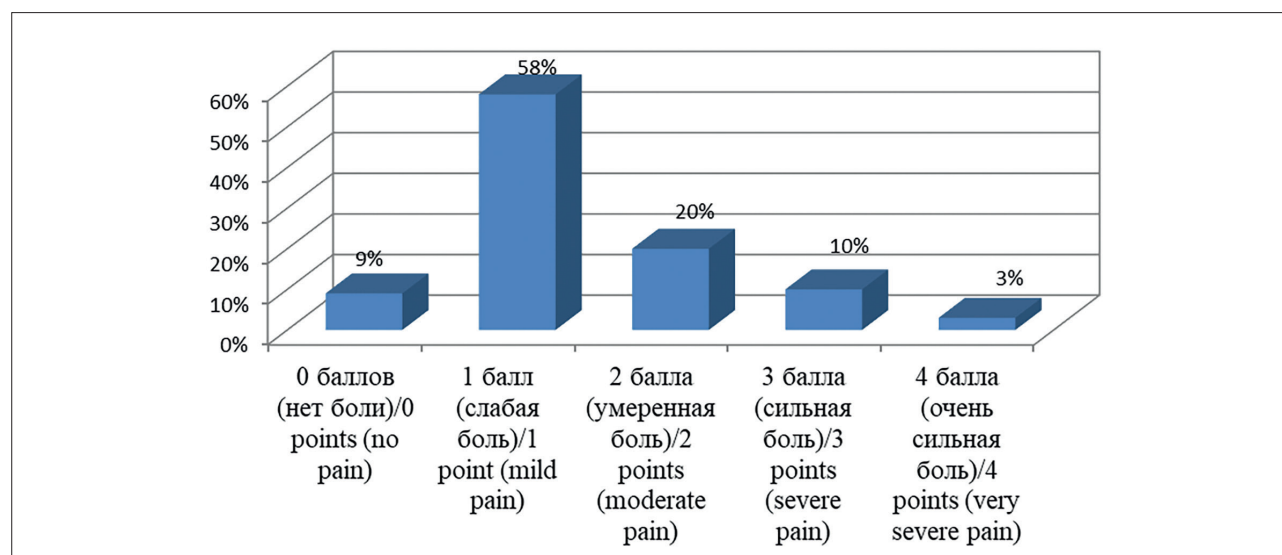**Fig. 1.** A verbal rating scale of pain syndrome intensity

Рис. 2. Интенсивность болевого синдрома по шкале вербальных оценок при проведении фотодинамической терапии (n=102)
Fig. 2. Pain syndrome intensity on the verbal rating scale during photodynamic therapy (n = 102)

(0–1 points) was observed in the treatment of basal cell skin cancer (89%), cancer of the oral and pharyngeal mucosa (100%), lower lip cancer (92%); nevertheless, in the treatment of squamous cell skin cancer, this indicator was 66%, and in PDT of leukoplakia and dysplasia of the oral mucosa, 78% (see Table).

This is due to the fact that in the treatment of patients with cancer of the oral mucosa and pharynx and cancer of the lower lip, we used conductive anesthesia in the majority of cases, which allowed us to achieve good control of the pain syndrome. With leukoplakia of the oral mucosa, a common process is often observed that involves various anatomical departments over a large area, making it difficult to perform conduction anesthesia and causing a relatively high level of pain impulses. A higher level of pain during PDT for squamous cell skin cancer is due to significantly larger lesion size and deep infiltration of the underlying tissues by the tumor compared to those observed in basal cell carcinoma (see Table).

The photosensitizer used did not affect the intensity of the pain syndrome, since in our study all the drugs used were classified as derivatives of e6 chlorin.

Severe pain during PDT leads to longer treatment time, as it is necessary to take breaks between the sessions of laser irradiation of the tumor. In 2 patients with stage II squamous cell carcinoma of the scalp, we were unable to complete the laser irradiation session due to severe pain and the refusal to continue the procedure with tramadol analgesia in combination with NSAIDs.

Despite the lack of recommendations for the use of local infiltration anesthesia in PDT, it was administered to 4 patients whose pain syndrome was not stopped by NSAIDs and opioid analgesics. The patients belonged to the 80+ age category and were treated for malignant neoplasms of the scalp or trunk of grade I–II. As an anesthetic, a 0.2% solution of ropivacaine was used, which was injected into the subcutaneous fat under the tumor, which did not produce a "lemon peel" effect. The pain syndrome was relieved, and the planned dose of laser radiation was administered. Complete tumor resorption was achieved in all 4 patients.

In 14 cases, we used conduction anesthesia for PDT of oropharyngeal tumors, since the treatment of neoplasms of this localization is accompanied by a significant pain
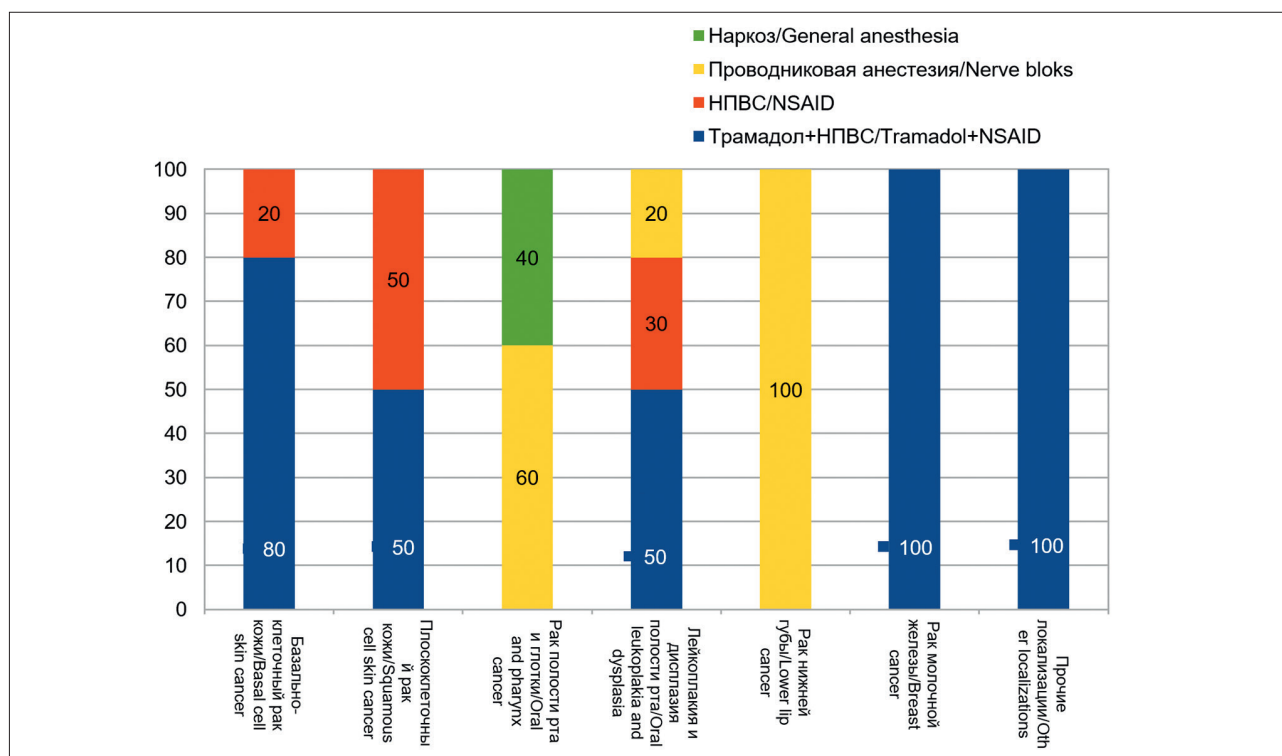
ORIGINAL ARTICLES

Рис. 3. Соотношение методов обезболивания при ФДТ различных нозологических форм опухолей
Fig. 3. Percentage of anesthesia methods used during PDT of various nosological forms of tumors

syndrome, which cannot be effectively controlled by the systemic administration of analgesics and sedatives. A 0.2% solution of ropivacaine was used as an anesthetic.

Ropivacaine is a long-acting local anesthetic of the amide type. It creates a reversible block of voltage-dependent sodium channels?and, therefore, prevents the generation of impulses in the endings of sensitive nerves and the conduction of impulses along nerve fibers. Conduction anesthesia does not interfere with blood supply and oxygenation of the tumor tissue, which is a necessary condition for the development of a photodynamic reaction. Ropivacaine action continues for at least 4–6 hours, which allows for excluding the period of the most severe pain impulses.

For cancer of the lower lip, mandibular anesthesia was used in combination with mental nerve block. Mandibular anesthesia was performed as follows. By index finger palpation, we determined the anterior edge of the lower jaw branch, inside of which the retromolar fossa was felt, and the temporal ridge behind it, which serves as a reference point for the needle injection site (Fig. 4). The injector was placed at the level of the premolars of the opposite side, the needle was inserted inside from the temporal ridge at a distance of 0.5–1 cm above the masticatory surface of the lower molars, directing the needle from the 2nd premolar of the opposite side outward and posteriorly until the contact with

the bone. Immediately after the puncture, 0.5 ml of anesthetic was administered to anesthetize the lingual nerve. After the needle was pushed deeper by 2 more cm and reached the bone groove, the remaining part of the anesthetic solution was injected to block the lower alveolar nerve [9, 10]. Mandibular anesthesia zone: the mucosa of the alveolar process of the lower jaw from molars to pre-molars of the corresponding side, the anterior 2/3 of the lateral surface of the tongue and half of the lower lip.

To perform mental anesthesia, the needle was inserted into the mucobuccal fold of the lower lip between the 2nd premolar and the 1st molar, and the needle was moved 1–2 cm to contact the bone, and the anesthetic was injected. Anesthesia zone: the frontal part of the soft tissues of the lower lip half, the mucous membrane of the mouth vestibule from the 2nd premolar to the 1st incisor of the opposite side, the mucous membrane of the alveolar process on the side of anesthesia.

For analgesia of the cheek mucosa, in addition to mandibular anesthesia, buccal nerve anesthesia or torus anesthesia was performed, and with the tumor localized in the upper posterior parts of the oral cavity (the posterior parts of the alveolar process of the upper jaw, the mucosa of the transitional fold and the upper posterior part of the cheek mucosa), tuberal anesthesia was performed.

Shinkarev S.A., Borisov V.A., Boldyrev S.V., Podolsky V.N., Abdurashidov Z.I., Zagadaev A.P., Klycheva O.N.
Possibilities of pain management during photodynamic therapy

ORIGINAL ARTICLES

Таблица
Исходные данные пациентов с отсутствием и слабой выраженностью болевого синдрома при фотодинамической терапии
Table
Initial data for patients with absent or mild pain syndrome during photodynamic therapy

Нозологическая форма Nosological form	Возраст (лет)* Age (years)*	Среднее число полей облучения (абс. ч.) Average number of irradiated areas	Средний размер очага (мм) Average focus size (mm)	Плотность дозы (Дж/см²)* Dose density (J/cm²)*	Плотность мощности (мВт/см²)* Power density (mW/cm²)*	Доля пациентов с оценкой болевого синдрома 0–1 балл (%) The proportion of patients with a pain score of 0–1 points
Базальноклеточный рак кожи (n=62) Basal cell skin cancer (n = 62)	74,5/78	2,6	23,8	293/300	524/509	89
Плоскоклеточный рак кожи (n=10) Squamous cell skin cancer (n = 10)	76,7/79	4,5	91,6	356/350	280/194	66
Рак слизистой оболочки полости рта и глотки (n=10) Oral and oropharynx mucosa cancer (n = 10)	61,3/64,5	3,0	22,5	282/290	401/380	100
Рак нижней губы (n=6) Lower lip cancer (n=6)	76,1/79,4	2,7	20,7	280/300	477/440	92
Лейкоплакия и дисплазия слизистой оболочки полости рта (n=8) Oral leukoplakia and dysplasia (n=8)	64,8/67	5,4	17,5	108/70	528/477	78

Примечание: * – среднее значение/медиана
Note: * – average value/median

Buccal nerve anesthesia was performed as follows. The needle was injected into the area of the anterior edge of the coronal process at the level of the masticatory surface of the upper molars into the cheek mucosa, directing the syringe from the opposite side. The needle was moved 1.0–1.5 cm to the anterior edge of the coronal process, and 1–2 ml of anesthetic was injected. Pain relief zone: the mucous membrane and the skin of the cheek.

When conducting torus anesthesia, anesthetic solution was injected into the region of the mandibular torus. It is located at the junction of the bony ridges coming from the coronoid and condylar processes, above and anteriorly from the bony growth of the lower jaw. The lower alveolar, lingual and buccal nerves are located below and inside the torus, surrounded by loose cellular tissue. When an anesthetic is administered to this area, these nerves can be blocked simultaneously. The syringe is placed on the molars of the opposite side. The needle is inserted into the groove formed by the lateral slope of the pterygomandibular fold and the cheek, at a distance of 0.5 cm below the masticatory surface of the upper 3rd molar (Fig. 5) [9, 10]. The needle is pushed 0.25–2 cm to the bone and 1.5–2 ml of anesthetic is injected (blocking the lower alveolar and buccal nerves). Move the needle a few millimeters in the opposite direction and inject 0.5–1.0 ml of anesthetic (blocking the lingual nerve). Area of anesthesia: all the teeth of the corresponding side, the bone tissue of the alveolar process of the lower jaw, the gum from the vestibular and lingual sides, the mucous membrane of the hyoid region, the front 2/3 of tongue, the skin and mucosa of the lower lip, the skin of the chin of the corresponding side, the mucosa and skin of the cheek.

Posterior superior alveolar nerve block was performed as follows: with the mouth half open, the cheek is drawn outwards with a spatula or dental mirror. The needle is placed at an angle of 45° to the crest of the alveolar

EMP

Shinkarev S.A., Borisov V.A., Boldyrev S.V., Podolsky V.N., Abdurashidov Z.I., Zagadaev A.P., Klycheva O.N.
Possibilities of pain management during photodynamic therapy

ORIGINAL ARTICLES

Рис. 4. Выполнение мандибулярной анестезии
Fig. 4. Mandibular anesthesia procedure

Рис. 5. Выполнение торусальной анестезии
Fig. 5. Torusal anesthesia procedure

Рис. 6. Выполнение туберальной анестезии
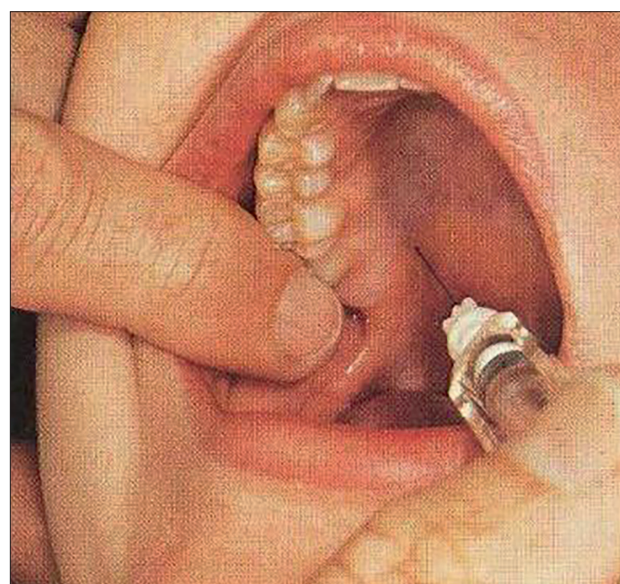**Fig. 6.** Tuberal anesthesia procedure

Рис. 7. Выполнение палатинальной анестезии
Fig. 7. Palatine anesthesia procedure

process, its bevel facing the bone. The needle is inserted at the level of the crown of the second molar or between the second and third molars into the mucous membrane, 0.5 cm outwards off from the mucobuccal fold (Fig. 6) [9, 10]. The needle is moved up, back and inwards to a depth of 2.5 cm, with the syringe directed outward so that the needle is always located as close to the bone as possible. To a certain extent, this prevents damage to the arteries, veins of the pterygoid venous plexus and hemorrhage into the surrounding tissues. After administration

of 2 ml of analgesic solution, anesthesia is achieved in 7–10 minutes.

In the absence of large molars, the zygoalveolar ridge that runs from the zygomatic process of the upper jaw to the outer surface of the alveolar process located at the level of the first molar is used as a benchmark. The needle is inserted behind the zygo-alveolar ridge, which corresponds to the middle of the crown of the missing second molar. The pain relief zone includes the periosteum of the alveolar process of the upper jaw and the mucous

Shinkarev S.A., Borisov V.A., Boldyrev S.V., Podolsky V.N., Abdurashidov Z.I., Zagadaev A.P., Klycheva O.N.
Possibilities of pain management during photodynamic therapy

ORIGINAL ARTICLES

membrane covering it in the area of these teeth on the side adjacent to the cheek; the mucous membrane and bone tissue of the posterior exterior wall of the maxillary sinus. The posterior border of the pain relief zone is constant. The anterior border may run along the middle of the crown of the first large molar or reach the middle of the first small molar.

For tumors of the anterior parts of the oral floor, mandibular anesthesia was performed on both sides with additional blocking of the lingual nerve in the area of the alveololingual groove. Lingual nerve anesthesia is administered as follows. With a spatula, the tongue is moved in the opposite direction and a needle is inserted into the mucous membrane of the maxillofacial groove at the level of the middle of the crown of the lower 3rd molar, where the nerve lies very superficially. 2 ml of anesthetic is administered. The analgesia zone: mucous membrane of the infrahyoid lobe, the anterior 2/3 of the tongue.

In the cases of tumor localization in the soft palate, palatinal anesthesia was performed. With this anesthesia, the greater palatine nerve is blocked in the area of the greater palatine foramen. For this purpose, the anesthetic must be injected into the area of the greater palatine foramen. It is located at the level of the middle of the 3rd molar crown, in the absence of the latter, posteriorly and internally from the 2nd molar, or 0.5 cm anteriorly from the border of the hard and soft palate. To determine the projection of the greater palatine foramen on the mucous membrane of the hard palate, it is necessary to draw two intersecting lines: one parallel to the border of the hard and soft palate at the level of the mid-crowns of the 3rd molars from the gingival margin to the midline of the upper jaw of the respective side (note that the maxilla is a paired bone), and the other through the middle of the first line and perpendicular to it (from front to back). The intersection point of these two lines will correspond to the projection of the greater palatine foramen.

The method of palatinal anesthesia is as follows. With the patient's mouth wide open, the needle is injected at a distance of 1 cm in front and inside of the projection of the palatine foramen on the mucous membrane, i.e.,

retreating to the midline (Fig. 7). The needle is pushed up, slightly posteriorly and outwards until it comes into contact with the bone. 0.5 ml of anesthetic is administered. Anesthesia is achieved after 3 to 5 minutes. Palatine anesthesia zone: the mucous membrane of the hard and soft palate, the alveolar process of the upper jaw on the palatine side from the 3rd molar to the middle of the canine crown [9, 10].

The pain syndrome among the group of patients with conduction anesthesia varied from 0 to 1 point; the planned dose of laser radiation was administered in full to all patients.

The indications for the use of anesthesia for PDT included recurrent tumors of the oral cavity and oropharynx in the presence of trismus of the masticatory muscles, postoperative scar deformation of the irradiation zone and difficult-to-reach anatomical localizations of the pathological process.

Conclusion

The severity of the pain syndrome during PDT depends on the histological form of the tumor, the extent of the lesion, and the method of anesthesia. The most pronounced pain syndrome is observed during PDT of squamous cell skin cancer, leukoplakia and dysplasia of the oral mucosa. NSAIDs alone or in combination with an opioid analgesic can effectively control pain in PDT of basal cell skin cancer in 89% of cases, and in PDT of squamous cell skin cancer in 66%. Conduction anesthesia allows you to relieve the pain syndrome during PDT of oropharyngeal tumors. Analgesia for PDT of visual localization tumors in elderly patients should be carried out with due consideration of the localization and prevalence of the pathological process, as well as concomitant pathology and the level of homeostasis compensation.

It is necessary to continue the development efforts aimed at solving the problem of pain relief during PDT. In order to unify approaches to choosing optimal methods of pain management in PDT, it is necessary to integrate the work of clinicians from different centers of the country and conduct randomized trials.

REFERENCES

1. Filonenko E.V., Serova L.G. Photodynamic therapy in clinical practice, Biomedical Photonics, 2016, T. 5, No. 2, pP. 26–37 (in Russ.).

2. Istomin Yu.P., Artemyeva T.P., Tzerkovsky D.A. Photodynamic therapy with photosensitizer photolon for oral leukoplakia, Biomedical Photonics, 2016, T. 5, No. 2, pP. 13–20 (in Russ.).

3. Klein A., Karrer S., Horner C., Werner A., Heinlin J., Zeman F., Koller M., Landthaler M., Szeimies R.-M., Gruber M., Graf B., Hansen E., Kerscher C. Comparing cold-air analgesia, systemically administered analgesia and scalp nerve blocks for pain management during photodynamic therapy for actinic keratosis of the scalp presenting as field cancerization: a randomized

ЛИТЕРАТУРА

1. Филоненко Е.В, Серова Л.Г. Фотодинамическая терапия в клинической практике // Biomedical Photonics. – 2016.– Т. 5, № 2. – С. 26–37.

2. Истомин Ю.П., Артемьева Т.П., Церковский Д.А. Фотодинамическая терапия лейкоплакии слизистой оболочки полости рта с фотосенсибилизатором фотолон // Biomedical Photonics. – 2016. – Т. 5, № 2. – С. 13–20.

3. Klein A., Karrer S., Horner C., Werner A., Heinlin J., Zeman F., Koller M., Landthaler M., Szeimies R.-M., Gruber M., Graf B., Hansen E., Kerscher C. Comparing cold-air analgesia, systemically administered analgesia and scalp nerve blocks for pain management

controlled trial, *British Journal of Dermatology*, 2015, vol. 173(1), pP. 192–200.

4. Fink C., Enk A., Gholam P. Photodynamic therapy - Aspects of pain , *JDDG: Journal Der Deutschen Dermatologischen Gesellschaft*, 2015, vol. 13(1), pP. 15–22.

5. Artemyeva T.P., Tzerkovsky D.A. Photodynamic therapy for vulvar leukoplakia, Biomedical Photonics, 2018, vol. 7, no. 4, pP. 4–10 (in Russ.).

6. Evstifeev S.V., Kulaev M.T., Rybkina O.A. Photodynamic therapy and diagnosis of lower lip cancer with photosense, *Fotodinami-cheskaya terapiya i fotodiagnostika*, 2014, vol. 3, no. 3, pP. 20–24 (in Russ.).

7. Ang J.M., Riaz I.B., Kamal M.U., Paragh G., Zeitouni N.C. Photodynamic therapy and pain: A systematic review, *Photodiagnosis Photodyn Ther*, 2017, pP. 308–344. doi: 10.1016/j.pdpdt.2017.07.002.

8. Ohnhaus E.E., Adler R. Methodological problems in the measurement of pain: a comparison between the verbal rating scale and the visual analogue scale, *Pain*, 1975, vol. 1(4), pP. 379–384.

9. *Rukovodstvo po khirurgicheskoi stomatologii i chelyustno-litsevoi khirurgii v 2-kh tomakh. T.2* [Guide to surgical dentistry and maxillofacial surgery in 2 volumes. Vol.2] by Bezrukov V.M., Pobustova T.G. as eds. Moscow, Meditsina Publ., 2000. 488 p.

10. *Khirurgicheskaya stomatologiya i chelyustno-litsevaya khirurgiya. Natsional'noe rukovodstvo* [Surgical dentistry and maxillofacial surgery. National guide] by Kulakov A.A., Robustova T.G., Nerobeev A.I. as eds. Moscow, GEOTAR-Media Publ., 2010. 928 p.

during photodynamic therapy for actinic keratosis of the scalp presenting as field cancerization: a randomized controlled trial // British Journal of Dermatology. – 2015. – vol. 173(1). – P. 192–200.

4. Fink C., Enk A., Gholam P. Photodynamic therapy - Aspects of pain management // JDDG: Journal Der Deutschen Dermatologischen Gesellschaft. – 2015. – Vol. 13(1). – P. 15–22.

5. Артемьева Т.П., Церковский Д.А. Фотодинамическая терапия при лейкоплакии вульвы // Biomedical Photonics. – 2018. – Т. 7, № 4. – С. 4–10.

6. Евстифеев С.В., Кулаев М.Т., Рыбкина О.А. Фотодинамическая терапия больных раком нижней губы // Фотодинамическая терапия и фотодиагностика. – 2014. – Т. 3, № 3. – С. 20–24.

7. Ang J.M., Riaz I.B., Kamal M.U., Paragh G., Zeitouni N.C. Photodynamic therapy and pain: A systematic review // Photodiagnosis Photodyn Ther. – 2017. – P. 308–344. doi: 10.1016/j.pdpdt.2017.07.002.

8. Ohnhaus E.E., Adler R. Methodological problems in the measurement of pain: a comparison between the verbal rating scale and the visual analogue scale // Pain. – 1975. – Vol. 1(4). – P. 379–384.

9. Руководство по хирургической стоматологии и челюстно-лицевой хирургии в 2-х томах. Т.2 / Под ред. В.М. Безрукова, Т.Г. Робустовой. – Изд. 2-е, перераб. и доп. – М.: Медицина, 2000. – 488 с.

10. Хирургическая стоматология и челюстно-лицевая хирургия. Национальное руководство / под ред. А.А. Кулакова, Т.Г. Робустовой, А.И. Неробеева. – М.: ГЕОТАР-Медиа, 2010. – 928 с.

EVALUATION OF STRONTIUM ALUMINATE PHOSPHORESCENT EFFECT ON BLOOD AS POTENTIAL LIGHT SOURCE FOR PHOTOTHERAPY

Heng Jie Choong, Nursakinah Suardi, Naser M. Ahmed
Universiti Sains Malaysia, School of Physics, 11800, Penang, Malaysia

Abstract

Phototherapy has shown its effect on cell stimulation and inhibition based on Arndt-Schulz model. Even though this therapeutic method has apparent effect, but it has limitations for epithelial application due to limitations on light penetration. Hence, with the ideology of fully overcoming this limitation, phosphorescent powder (strontium aluminate) is proposed as the potential light source that emitting photon from inside the body for phototherapy purposes. The strontium aluminate powder used in the experiment has the highest peak absorption at wavelength around 650 nm and lowest at around 350 nm. According to FESEM images, the powder has the particle size varies from 10 to 50 μm at cubic phase. The assessment is done by studying the effect on erythrocyte after blood plasma is irradiated by strontium aluminate powder's photon. The powder luminesces with a maximum at 491.5 nm when pumped with 473 nm laser at 100 mW in fixed amount of 0.005±0.001 g. Later, it is mixed with centrifuged blood plasma for a predetermined time period (5, 10, 15, and 20 minutes). From this study, it shows that 5 minutes irradiation is the optimum period for erythrocyte in term of morphology enhancement and increase of UV-visible absorption spectrum with at least 21% in comparing with control blood. While the significant increment located at wavelengths 340 nm and 414 nm with both increased by 54% and 41%, respectively. However, for 10 minutes and beyond, the irradiation leads to morphology deterioration while the UV-visible spectrum decrement starts at 15 minutes and beyond. In conjunction, a comparison between blood plasma that either interacted with powder emitting photon or powder with no emission shows that photon emission plays a role in the phototherapy effect.

Keywords: phototherapy, phosphorescent, red blood cells, UV-visible spectroscopy, self-illuminated, laser.

Contacts: Heng Jie Choong, e-mail: choonghengjie@yahoo.com
Nursakinah Suardi, e-mail: nsakinahsuardi@usm.my

ОЦЕНКА АЛЮМИНАТА СТРОНЦИЯ КАК ПОТЕНЦИАЛЬНОГО ИСТОЧНИКА СВЕТА ДЛЯ ФОТОТЕРАПИИ ПО ЕГО ФОСФОРЕСЦЕНТНОМУ ДЕЙСТВИЮ НА КРОВЬ

Heng Jie Choong, Nursakinah Suardi, Naser M. Ahmed
Научный университет Малайзии, Малайзия

Резюме

Несмотря на доказанную эффективность фототерапии, у этого метода есть ограничения для эпителиального применения из-за незначительного проникновения света. Авторами предложен фосфоресцирующий порошок (алюминат стронция) в качестве потенциального источника света, излучающего фотоны изнутри тела для целей фототерапии. Порошок алюмината стронция, использованный в эксперименте, имеет самое высокое пиковое поглощение при длине волны около 650 нм и самое низкое при длине волны около 350 нм. Согласно изображениям автоэлектронной сканирующей микроскопии, порошок имеет размер частиц от 10 до 50 мкм в кубической фазе. Оценка эффективности фототерапии с предложенным соединением проведена путем изучения воздействия на эритроциты облученной порошком плазмы крови. Фосфоресценция порошка с фиксированный массой 0,005 ± 0,001 г имеет максимум на длине волны 491,5 нм при накачке лазером с длиной волны 473 нм с мощностью 100 мВт. Затем его смешивают с центрифугированной плазмой крови в течение определенного периода времени (5, 10, 15 и 20 мин). Полученные результаты демонстрируют, что 5-минутное облучение является оптимальным периодом для эритроцитов с точки зрения улучшения морфологии и увеличения спектра поглощения УФ-видимой области по крайней мере на 21% по сравнению с контрольной кровью. При этом значительный прирост приходится на длины волн 340 нм и 414 нм, которые увеличиваются на 54% и 41% соответственно. Однако, для 10 мин и более облучение вызывает ухудшение морфологии, в то время как УФ-видимый спектр уменьшается начиная с 15 мин и позже. В связи с этим изучается сравнение плазмы крови, которая взаимодействовала с фосфоресцирующим порошком, с нефосфоресцирующим порошком, чтобы показать, что излучение играет роль в создании эффекта фототерапии.

ORIGINAL ARTICLES

Контакты: Heng Jie Choong, e-mail: choonghengjie@yahoo.com
Nursakinah Suardi, e-mail: nsakinahsuardi@usm.my

Introduction

Phototherapy utilized light to conduct treatment with different light source and variation of parameters such as wavelength, irradiance, pulse structure, coherence, and polarization [1–3]. Initially, laser is widely used as it is thought that the monochromatic and coherence of laser would give extra benefit for treatment. This thought was no longer hold as similar effect is observed by using monochromatic light source like Light Emitting Diodes (LEDs) [4]. The respond of cells, either stimulation or inhibition, is depended on the output power of light which can be described through Arndt-Schulz curve and Arndt-Schulz model. The cells would be stimulated at certain threshold and inhibition is promoted beyond the threshold. From Arndt-Schulz model the parameters for the threshold are wavelength of light, irradiance of light, and the period of irradiation. The absolute Arndt-Schulz model is associated with parameters like wavelengths, tissue types, redox states, and different pulse parameters [3, 5–7].

Several experiments were conducted to observe the phototherapy effect by using different light sources while wavelength of light, irradiance, and exposure time remains the same. The results showed that similar effects can be observed even though different light sources were used [1, 2, 8]. Among the phototherapy treatment, phototherapy towards blood able to show significant effect. A study conducted by Siti Sakinah Mohd Fuad et al. showed that the RBCs of human blood would denature and forming echinocytes after irradiated by 589 nm yellow laser. The formation of echinocytes was caused by the loss of water and potassium, which decreases the generation of Adenosine Triphosphate (ATP). Concurrently, the RBCs' light absorption showed increment after irradiation for 10 minutes till 40 minutes. The decrement of absorbance was observed after the irradiation extended to 50 minutes and beyond. This corresponds to biphasic response of having two, either good or bad, reaction oxygen species (ROS). Mitochondrial would be stimulated on electron transport, which increases ATP production for good ROS. At the same time, the cell would signal and activate redox-sensitive transcription factors. On the contrary, bad ROS occur as the dose increases and lead to the damaging of mitochondria and apoptosis [9]. Another study conducted by Kujawa et al. demonstrated a visible effect on RBCs' ATPase activities and membrane structure after irradiated with near infrared (810 nm) laser. The irradiation-induced modulation of RBCs membrane which could change the activity of membrane ion pumps and ion flows [10]. The effect towards RBCs can be induced through blood plasma. Mustafa et al. conducted a study on erythrocyte sedimentation rate (EST) after irradiated with low-level laser. The study showed that effective reduction of ESR appeared after the irradiation of laser with a dose of 72 J/cm^2 at wavelength of 405 nm. Besides, their study showed that whole blood ESR reduction is greatly reduced to less than 51% (from 15±3.7 mm/h to 7.6±2.3 mm/h) in comparison between separated RBCs resuspended in irradiated plasma and separated RBCs resuspended in non-irradiated plasma. Hence, this study suggested that the whole blood ESR effect is mainly induced by the plasma composition [11].

Due to the limitation of light penetration towards the region of interest within the body, phototherapy has been limited for epithelial application. Attempts have been taken by introducing penetrating light in the red or near infrared range, for brain photobiomodulation to relieve brain disorders [12–16]. However, the penetration is still limited to a certain depth depending on the anatomical region. For instance, 808 nm light source has penetration to depth about 40 mm to 50 mm [14, 17, 18]. Alternatively, intracranial method is an approach to overcome the limitation by directly deliver light to the brain with light-optical fiber device. However, this method is associated with risk as minimal surgical stereotactic procedure is needed to insert light-optical device within the brain [12].

Hence, in conjunction to overcome the limitation, it is proposed to use light source, like phosphorescent powder, that could emit light after traveling to the region of interest within the body itself. This paper is assessing phosphorescent powder (strontium aluminate) as the potential light source for phototherapy through *in vitro* blood phototherapy by irradiating blood plasma with RBCs morphology and absorbance spectrum being studied.

Materials and Methods

Characterization of strontium aluminate powder
The absorption of strontium aluminate was evaluated using UV-Visible spectrophotometer at the

Heng Jie Choong, Nursakinah Suardi, Naser M. Ahmed
Evaluation of strontium aluminate phosphorescent effect on blood as potential light source for phototherapy

ORIGINAL ARTICLES

BMP

range of 200 nm to 800 nm. Emission spectroscopy was used to evaluate the emission of strontium aluminate at the range of 380 nm to 780 nm. XRD was performed in comparison with database compounds. Particle size and crystal structure was observed via FESEM images at 500, 5000, and 10,000 times of magnification.

Preparation of strontium aluminate powder

Strontium aluminate powder used for this study emitted greenish-blue light at the dominant wavelength of 491.5 nm. The powder was transferred to two plain test tubes with each at the weight of 0.005±0.001 g. One of the tubes placed in a dark room to ensure no/minimum exposure of light to prevent charging powder. The second tube was irradiated with 473 nm single longitudinal mode beam blue laser at a constant output of 100 mW for ~15 minutes. Laser was placed at focus distance (~16 cm) when irradiating the powder. The irradiation was done with laser to ensure the powder charged at known constant power, light energy, and period of charging.

Preparation of blood samples

Blood samples of 3 ml were collected randomly from a wide range of patients with unknown information on blood counts and patients' gender. The patients were generally declared fit outpatients at the age group of 20 years old to 70 years old. The EDTA blood sample was partitioned to three aliquots with 1 ml on each tube. One of the aliquots served as control (untreated). The other two were centrifuged to separate blood plasma and RBCs which the plasma later mixed with strontium aluminate powder for interaction.

Irradiation to blood plasma

The centrifuged blood plasmas were mixed with two tubed strontium aluminate powders, respectively. One of the tubed powders emitted photons when interacting with blood plasma. At the same time, the second powders emitted no/minimum light when interacting with blood plasma. Both blood plasmas with powder content interacted for 5, 10, 15, and 20 minutes. Later, the plasmas were mixed back to their respective RBCs for interaction at ~22 minutes.

Observation of RBCs morphology and absorbance spectrum

The morphology of RBCs was observed via an optical microscope at 40 times magnification after blood smearing with a thin film of streaked blood. Blood smearing was done by having a portion of blood dropped near the frosted end of a clean glass slide and second glass slide as a spreader. The absorbance of washed RBCs was measured using a UV-Visible spectrophotometer at the range of 300 nm to 800 nm.

Ethical consideration

This study is ethically approved by Universiti Sains Malaysia Research Ethics Committee under the study code of USM/JEPeM/16060208.

Results and discussion

Optical and structural properties of strontium aluminate powder

The absorbance spectrum for strontium aluminate powder in Fig. 1 shows that it is able to absorb a wide range of spectrum from 200 nm to 800 nm. The absorption appears to be highest at the peak at around 650 nm.
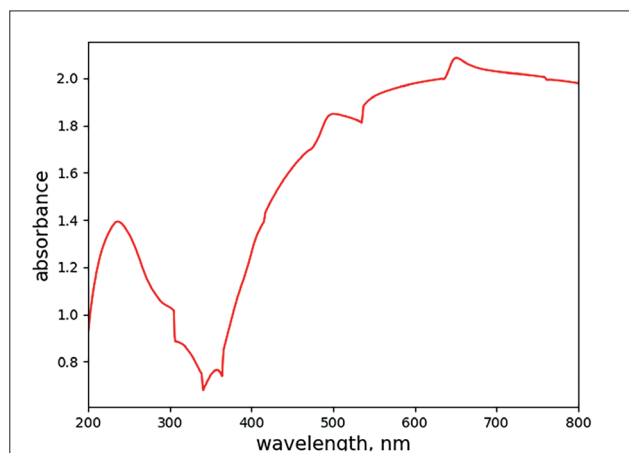

Fig. 1. Absorbance spectrum of strontium aluminate at wavelength of 200 nm to 800 nm. The highest absorption located at around 650 nm and lowest at around 350 nm
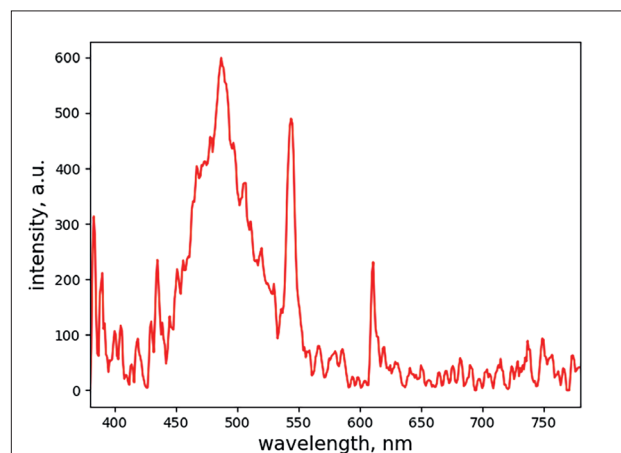**Рис. 1.** Спектр поглощения алюмината стронция в интервале длин волн от 200 нм до 800 нм

Fig. 2. Emission spectrum of strontium aluminate at wavelength of 380 nm to 780 nm after being irradiated with 473 nm laser. The dominant peak located at 491.5 nm
Рис. 2. Спектр излучения алюмината стронция в интервале длин волн от 380 нм до 780 нм после облучения лазером при длине волны 473 нм
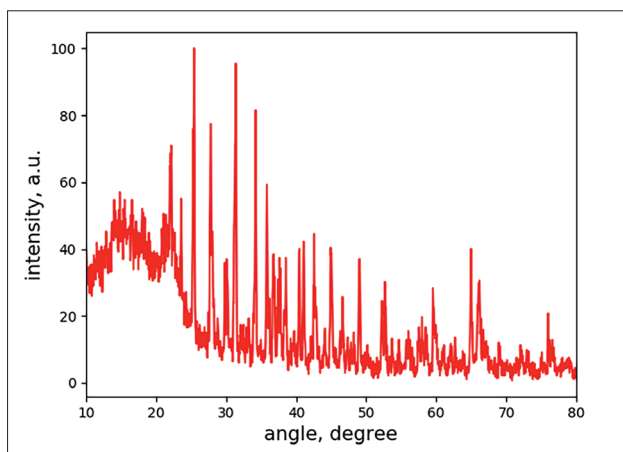
Fig. 3. XRD of strontium aluminate powder
Рис. 3. Рентгеноструктурный анализ порошка алюмината стронция

At the same time, the minimum absorption appears at wavelength around 350 nm, which is represented with a trough. With the presence of the trough, it caused another appearance of a peak at a wavelength of around 250 nm. Notice that the 250 nm peak's absorption is still not as high as other wavelengths ranging from 400 nm to 800 nm.

Simultaneously, the emission spectrum of strontium aluminate powder has a dominant peak at 491.5 nm, as shown in Fig. 2. Hence, with this known information, 473 nm laser was selected as the light source to charge strontium aluminate. This is due to higher light energy is required to allow strontium aluminate powder emitting 491.5 nm cyan (greenish-blue) light [19].

The XRD pattern of the powder is shown in Fig. 3. After comparing with database's (reference code: 00–052–1876) intensity peaks, it shows that the powder is potentially containing strontium, aluminum, and oxygen. In this pattern, the peaks can be indexed based on space group of PMMA with the number of 51 and orthorhombic crystal system. The orthorhombic system can be viewed at the FESEM images shown in Fig. 4a with 10,000 times of magnification. The crystal appears in pack with the size of approximately 4 µm. Fig. 4b and 4c suggested that the particle size varies from 10 µm to 50 µm at cubic phase.

Reaction of blood towards strontium aluminate

Within the absorbance spectrum of RBCs, there are four obvious peaks along the spectrum at wavelength ranging from 300 nm to 800 nm as shown in Fig. 5. The first peak appears at 340 nm, which indicates the maximum carbohydrate metabolism of blood caused by the structural changes of Nicotinamide Adenine Dinucleotide (NAD) into NADH and Nicotinamide Adenine Dinucleotide Phosphate (NADP) into NADPH through the reduction process. The other three peaks are visible at 414, 542, and 576 nm due to d-f transition of CO-oxyhemoglobin. The intensity of absorbance is linearly dependent by the concentration of solutes within blood samples after irradiation [9, 20, 21].

As shown in Fig. 5, after the blood plasma interacted with the strontium aluminate powder, there is an obvious increment of absorbance intensity with respect to control blood, especially at 340 nm. However, the intensity decrements when photons are emitted from powder, which acts as a light source. This has depicted a biphasic response (hormesis) given off by RBCs as the solely addi-
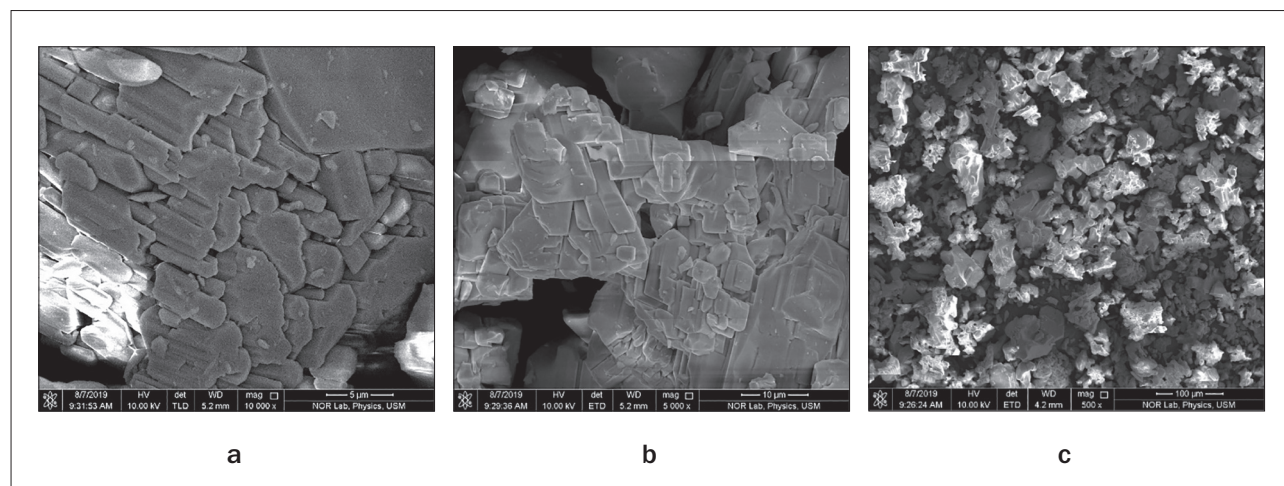

a   b   c

Fig. 4. FESEM images of strontium aluminate with difference magnification:
    a – 10,000 times magnification;
    b – 5,000 times magnification;
    c – 500 times magnification
Рис. 4. Снимки алюмината стронция, полученные на сканирующем электронном микроскопе при различном увеличении:
    a – 10,000-кратное увеличение;
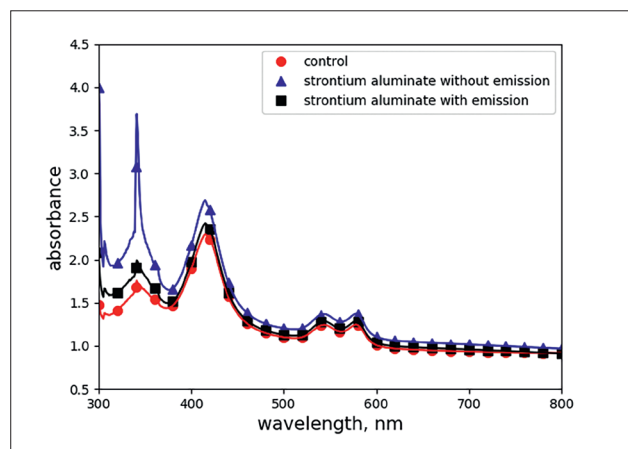   b – 5,000-кратное увеличение;
    c – 500-кратное увеличение

Fig. 5. Absorbance spectrum of RBCs at three conditions (control blood sample, blood sample with plasma interacted with no emission from strontium aluminate powder, and blood sample with plasma interacted with photon emission from powder) at the range of 300 to 800 nm

Рис. 5. Спектр поглощения эритроцитов в трех условиях (контрольная проба крови, проба крови с плазмой, взаимодействующей с неизлучающим порошком алюмината стронция, и проба крови с плазмой, взаимодействующей с фосфоресцирующим порошком) в диапазоне от 300 до 800 нм

tion of powder, either photon emitting or not, changes the environment factor of blood [5–7]. The changes in intensity are associated with the variability of coenzyme in conjunction with echinocytes [22].

Shown in Fig. 6 is the morphology of RBCs with the presence of echinocytes labeled. The number of echinocytes increases along with the present powder and further increased as powder emitting photon. This suggested that the increment at 340 *nm* is due to the production of NADPH in preventing globin from denaturing [22]. Concurrently, a further increase of echinocytes de-
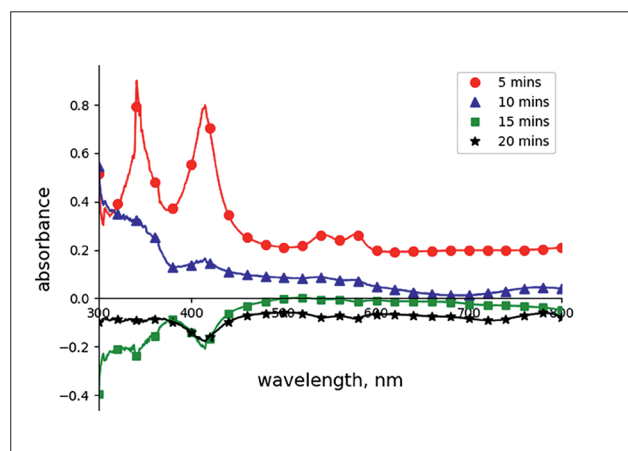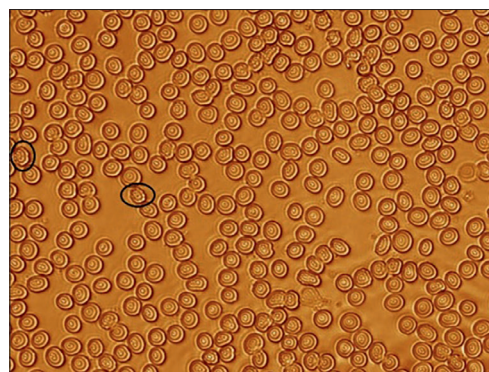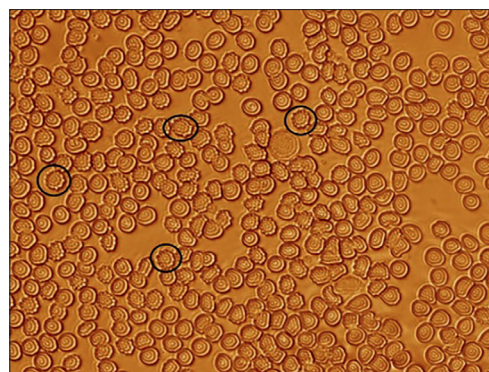

Fig. 7. Absorbance spectrum of RBCs after interacted with photon emitting strontium aluminate powder for 5, 10, 15, and 20 minutes
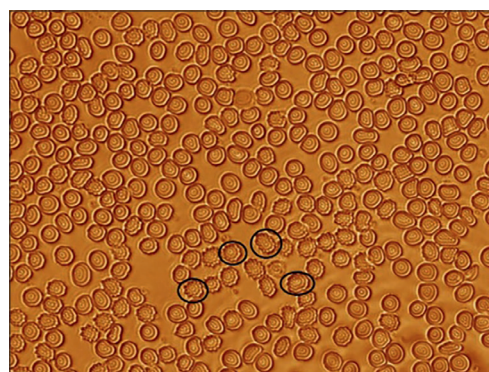
Рис. 7. Спектр поглощения эритроцитов после взаимодействия с фосфоресцирующимм порошком алюмината стронция в течение 5, 10, 15 и 20 мин

Fig. 6. RBCs morphology for control blood samples and blood samples that the blood plasma interacted with strontium aluminate powder (photon emitting and no photon emitting) for 5 minutes. Some presence of echinocytes are indicated with circles:

a – control blood samples;
b – blood plasma interacted with photon emitting strontium aluminate powder;
c – blood plasma interacted with no photon emitting strontium aluminate powder

Рис. 6. Морфология эритроцитов для контрольных образцов крови и образцов крови после взаимодействия плазмы с порошком алюмината стронция:

a – контрольные образцы крови;
b – после взаимодействия плазмы крови с фосфоресцирующим порошком алюмината стронция;
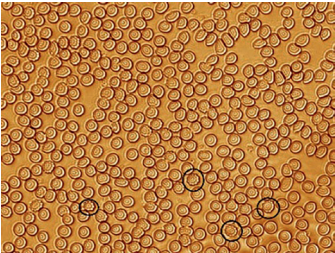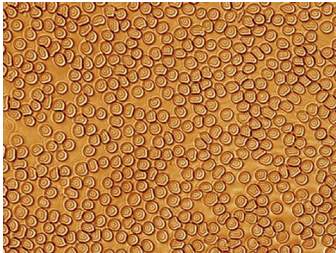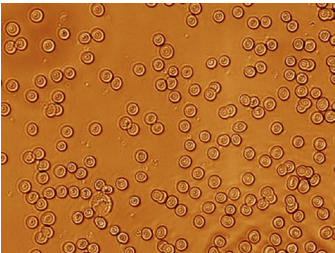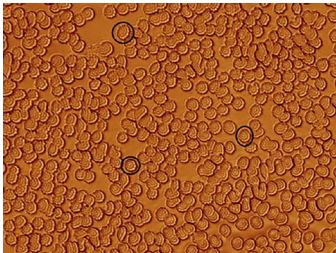c – после взаимодействия плазмы крови с неизлучающим порошком алюмината стронция

ORIGINAL ARTICLES
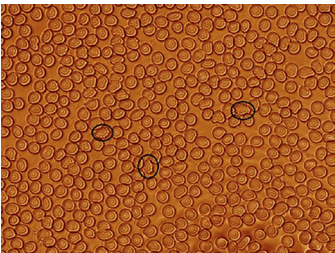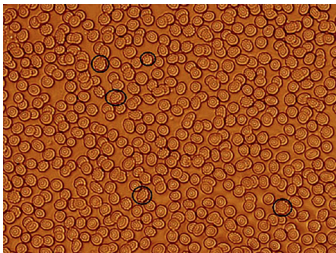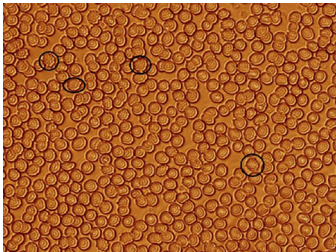
Period, minutes	Control Blood Контрольные образцы крови	Irradiated Blood Облученная кровь
5	 a(i): Before irradiation some echinocytes are presented. a(i): До облучения обнаруживаются эхиноциты	 a(ii): After irradiation no echinocyte is observed. a(ii): После облучения эхиноциты отсутствуют
10	 b(i): Before irradiation no echinocyte is observed. b(i): До облучения эхиноциты отсутствуют	 b(ii): After irradiation echinocytes are observed. b(ii): После облучения обнаруживаются эхиноциты
15	 c(i): Before irradiation small number of echinocytes are observed. c(i): До облучения обнаруживается незначительное количество эхиноцитов	 c(ii): After irradiation increase number of echinocytes are observed. c(ii): После облучения количество эхиноцитов увеличено
20	 d(i): Before irradiation small number of echinocytes are observed. d(i): До облучения обнаруживается незначительное количество эхиноцитов	 d(ii): After irradiation increase number of echinocytes are observed. d(ii): После облучения количество эхиноцитов увеличено

Fig. 8. RBCs morphology for control blood and blood, which has its plasma interact with photon emitting strontium aluminate. The interaction (irradiation) period is shown in the "Period" column with values of 5, 10, 15, and 20 minutes. Some echinocytes are indicated with circles

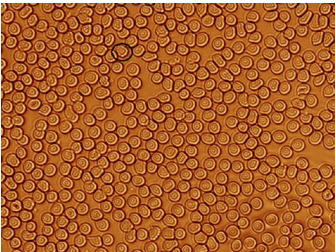**Рис. 8.** Морфология эритроцитов для контроля крови и крови, в плазме которой происходит взаимодействие с испущенными алюминатом стронция фотонами. Период взаимодействия (облучения) показан в столбце "период", который включает в себя 5, 10, 15 и 20 минут. Некоторые эхиноциты обозначены кружочками

Heng Jie Choong, Nursakinah Suardi, Naser M. Ahmed
Evaluation of strontium aluminate phosphorescent effect on blood as potential light source for phototherapy

ORIGINAL ARTICLES
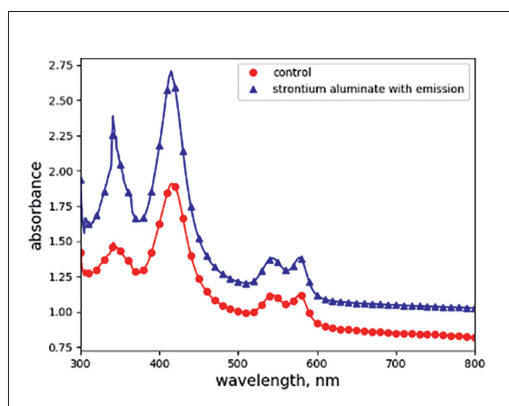
(a): Blood plasma irradiated for **5 minutes**. Absorbance for irradiated blood has increased compare to the control blood.
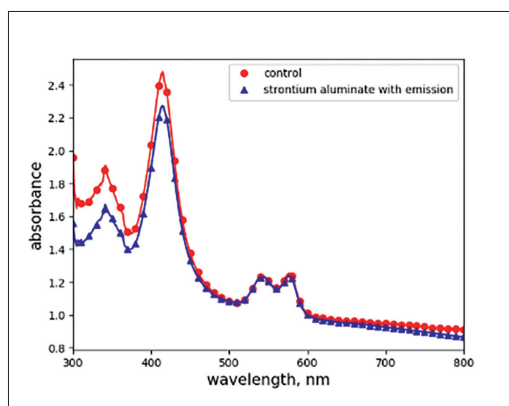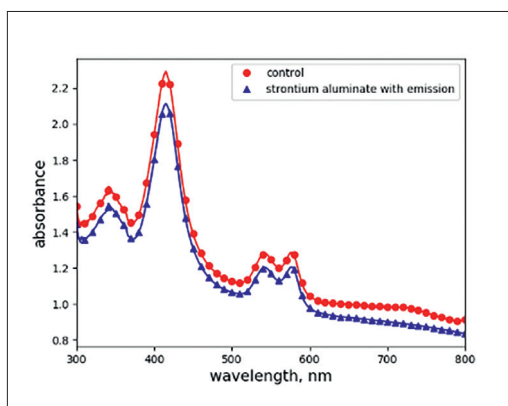(a): Плазму крови облучали в течение **5 мин**. Поглощение облученной крови увеличилось по сравнению с контрольной кровью
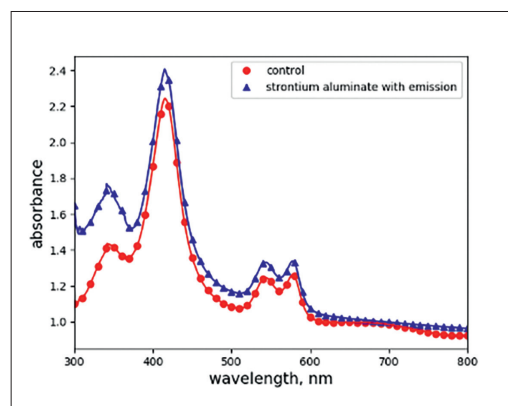
(b): Blood plasma irradiated for **10 minutes**. Absorbance for irradiated blood has slightly increased compare to the control blood.
(b): Плазму крови облучали в течение **10 мин.** Поглощение для облученной крови несколько увеличилось по сравнению с контрольной кровью.

(c): Blood plasma irradiated for **15 minutes**. Absorbance for irradiated blood has decreased compare to the control blood.
(c): Плазму крови облучали в течение **15 мин**. Поглощение для облученной крови уменьшилось по сравнению с контрольной кровью.

(d): Blood plasma irradiated for **20 minutes**. Absorbance for irradiated blood has decreased compare to the control blood.
(d): Плазму крови облучали в течение **20 мин**. Поглощение для облученной крови уменьшилось по сравнению с контрольной кровью.

Fig. 9. Absorbance spectrum of RBCs for irradiated blood samples and control blood samples. The period of irradiation is stated at each Fig.
Рис. 9. Спектр поглощения эритроцитов для облученных образцов крови и контрольных образцов крови. Период облучения указан на каждом графике

creases the production of ATP [23]. Notice that the effect is observable even though only blood plasma is irradiated. This phenomenon is known as the bystander effect, in which the effect towards RBCs is induced by the changes of blood plasma (medium) after interaction with the powder [24].

Analyzation of absorbance and morphology of RBCs
Shown in Fig. 7 is the absorbance after the blood plasma has been irradiated by photon emitted from strontium aluminate powder for 5, 10, 15, and 20 minutes. The irradiance of powder is kept at constant by having a constant amount in terms of weight and laser power when irradiated. The absorbance appears to be highest after 5 minutes of irradiation and starts to decrease beyond that. This relationship coincides with Arndt-Schulz model, which suggests 5 minutes irradiation is the optimum for stimulation, with the inhibition after 5 minutes.

Based on the RBCs morphology between control blood and irradiated blood, the chemical changes can

be studied. From the morphologies shown in Fig. 8, the morphology has enhanced with the restoration of discocyte state from echinocyte. This restoration can normally be done by in vitro suspending normal plasma, albumin, glucose, gelatin, polyvinyl-pyrrolidine and fixatives such as glutaraldehyde, osmic acid, etc. [25]. This enhancement is observed after 5 minutes of irradiation. However, denaturing occurs after 10 minutes irradiation and beyond.

The presence of echinocytes suggested the decrease of ATP caused by loss of water and potassium in RBCs. Hence, with the improvement of morphology (decrease number of echinocytes) the ATP would be increased [22, 23]. However, at 10 minutes irradiation the denaturing may have underwent the production of NADPH to reduce oxidized glutathione into glutathione with the aim of preventing the denaturing of globin within RBCs [22]. The variation of solutes is shown in conjunction with the absorbance spectrum, as displayed in Fig. 7 [21–23]. The absorbance spectrum in Fig. 7 is obtained by having the subtraction between the irradiated blood's absorbance spectrum (abs_{irr}) with control blood's absorbance spectrum ($abs_{control}$). This is done to examine the sole effect of photon towards blood by eliminating the possible inherent illness from the patients [26]. The equation representation is as followed: $abs_{irr} - abs_{control}$. Individual absorbance spectrums are shown in Fig. 9 for further reference. Notice that the decrease in abs_{irr} with $abs_{control}$ as a reference that results in a negative absorbance shown in Fig. 7.

Conclusion

There is an obvious effect on blood using solely phosphorescent powder as light source for phototherapy. Even though the presence of phosphorescent powder changes the environment factor of blood, which induces the blood to respond with a process known as hormesis; photons have also played a role in changing the environment factor, as shown in section 3.2 Reaction of blood towards strontium aluminate. The results show that the optimum period of irradiation is 5 minutes with the improvement in RBCs morphology and increment in RBCs absorbance. Irradiation of 10 minutes and beyond induces inhibition of RBCs with a deterioration of morphology and decrement of absorbance. Bystander effect is observed in this study as RBCs are affected, although only blood plasma is irradiated. For future improvement, it is recommended to introduce magnetic-organic phosphorescent material with manipulatable photon emission for in-vivo usage. With this ideology, the material can be magnetically localized at the region of interest within the body, and can later carry out phototherapy. The controllable photon emission is integrated to avoid any unnecessary irradiation at the unintended area during treatment.

Acknowledgement

REFERENCES

1. Le Duff F. et al. 308-nm excimer lamp vs. 308-nm excimer laser for treating vitiligo: A randomized study, *Br. J. Dermatol*, 2010, vol. 163, № 1, pp. 188–192.
2. Seidman D.S. et al. A prospective randomized controlled study of phototherapy using blue and blue-green light-emitting devices, and conventional halogen-quartz phototherapy, *J. Perinatol*, 2003, vol. 23, № 2, pp. 123–127.
3. Chung H. et al. The nuts and bolts of low-level laser (Light) therapy, *Ann. Biomed. Eng,* 2012, vol. 40, № 2, pp. 516–533.
4. De Freitas L.F., Hamblin M.R. Proposed Mechanisms of Photobiomodulation or Low-Level Light Therapy, *IEEE J. Sel. ToP. Quantum Electron*, 2016, vol. 22, № 3, pp. 1–37.
5. Hamblin M.R. et al. Biphasic dose response in low level light therapy - an update, *Dose-Response,* 2011, vol. 9, № 4, pp. 602–618.
6. Mattson M.P. Hormesis defined, *Ageing Res. Rev*, 2008, vol. 7, № 1, pp. 1–7.
7. Sommer A.P. et al. Biostimulatory Windows in Low-Intensity Laser Activation: Lasers, Scanners, and NASA's Light-Emitting Diode Array System, *J. Clin. Laser Med. Surg*, 2002, vol. 19, № 1, pp. 29–33.
8. Chen H. et al. Quantum dot light emitting devices for photomedical applications, *J. Soc. Inf. Disp*, 2017, vol. 25, № 3, pp. 177–184.
9. Mohd Fuad S.S., Suardi N., Mustafa I.S. In Vitro UV-Visible Spectroscopy Study of Yellow Laser Irradiation on Human Blood, *J. Phys. Conf. Ser*, 2018, vol. 995, № 1.
10. Kujawa J. et al. Effect of Low-Intensity (3.75–25 J/cm^2) Near-Infrared (810 nm) Laser Radiation on Red Blood Cell ATPase

ЛИТЕРАТУРА

1. Le Duff F. et al. 308-nm excimer lamp vs. 308-nm excimer laser for treating vitiligo: A randomized study // Br. J. Dermatol. – 2010. – Vol. 163, № 1. – P. 188–192.
2. Seidman D.S. et al. A prospective randomized controlled study of phototherapy using blue and blue-green light-emitting devices, and conventional halogen-quartz phototherapy // J. Perinatol. – 2003. – Vol. 23, № 2. – P. 123–127.
3. Chung H. et al. The nuts and bolts of low-level laser (Light) therapy // Ann. Biomed. Eng. – 2012. – Vol. 40, № 2. – P. 516–533.
4. De Freitas L.F., Hamblin M.R. Proposed Mechanisms of Photobiomodulation or Low-Level Light Therapy // IEEE J. Sel. ToP. Quantum Electron. – 2016. – Vol. 22, № 3. – P. 1–37.
5. Hamblin M.R. et al. Biphasic dose response in low level light therapy - an update // Dose-Response. – 2011. – Vol. 9, № 4. – P. 602–618.
6. Mattson M.P. Hormesis defined // Ageing Res. Rev. – 2008. – Vol. 7, № 1. – P. 1–7.
7. Sommer A.P. et al. Biostimulatory Windows in Low-Intensity Laser Activation: Lasers, Scanners, and NASA's Light-Emitting Diode Array System // J. Clin. Laser Med. Surg. – 2002. – Vol. 19, № 1. – P. 29–33.
8. 8Chen H. et al. Quantum dot light emitting devices for photomedical applications // J. Soc. Inf. Disp. – 2017. – Vol. 25, № 3. – P. 177–184.
9. Mohd Fuad S.S., Suardi N., Mustafa I.S. In Vitro UV-Visible Spectroscopy Study of Yellow Laser Irradiation on Human Blood // J. Phys. Conf. Ser. – 2018. – Vol. 995, № 1.

Activities and Membrane Structure, *J. Clin. Laser Med. Surg*, 2004, vol. 22, № 2, pp. 111–117.

11. Al Musawi M.S. et al. Erythrocyte sedimentation rate of human blood exposed to low-level laser, *Lasers Med. Sci. Lasers in Medical Science*, 2016, vol. 31, № 6, pp. 1195–1201.

12. Mitrofanis J. et al. The potential of light therapy in Parkinson's disease, *ChronoPhysiology Ther*, 2014, February.

13. Shaw V.E. et al. Neuroprotection of midbrain dopaminergic cells in MPTP-treated mice after near-infrared light treatment, *J. ComP. Neurol*, 2010, vol. 518, № 1, pp. 25–40.

14. Hamblin M.R. Shining light on the head: Photobiomodulation for brain disorders, *BBA Clin. The Author*, 2016, vol. 6, pp. 113–124.

15. Lapchak P.A., Wei J., Zivin J.A. Transcranial Infrared Laser Therapy Improves Clinical Rating Scores After Embolic Strokes in Rabbits, 2004, pp. 1985–1988.

16. Sadeh M. et al. Low-Level Laser Therapy Applied Transcranially to Rats After Induction of Stroke Significantly Reduces Long-Term, 2006, pp. 2620–2624.

17. Jagdeo J.R. et al. Transcranial Red and Near Infrared Light Transmission in a Cadaveric Model, *PLoS One*, 2012, vol. 7, № 10, pp. 1–10.

18. Tedford C.E. et al. Quantitative analysis of transcranial and intraparenchymal light penetration in human cadaver brain tissue, *Lasers Surg. Med*, 2015, vol. 47, № 4, pp. 312–322.

19. Baryshnikov G., Minaev B., Ågren H. Theory and Calculation of the Phosphorescence Phenomenon, *Chem. Rev*, 2017, vol. 117, № 9, pp. 6500–6537.

20. Mattley Y. et al. Blood characterization using UV/vis spectroscopy, 1995, vol. 2388, pp. 462–470.

21. Soltani S., Ojaghi A., Robles F.E. Deep UV dispersion and absorption spectroscopy of biomolecules, *Biomed. Opt. Express*, 2019, vol. 10, № 2, pp. 487.

22. Brown K.A. Erythrocyte metabolism and enzyme defects, *Lab. Med*, 1996, vol. 27, № 5, pp. 329–333.

23. Lynch E.C. Peripheral Blood Smear- Edward Lynch, *Clinical Methods: The History, Physical, and Laboratory Examiniations. 3rd ed. Butterworth Publishers*, 1990, pp. 732–734.

24. Paul A. et al. The bystander effect in optically trapped red blood cells due to plasmodium falciparum infection, *Trans. R. Soc. TroP. Med. Hyg*, 2013, vol. 107, № 4, pp. 220–223.

25. Marcel B., Lawrence S. L. The Discocyte-Echinocyte Equilibrium of the Normal and Pathologic Red Cell, 1970., vol. 36, № 3, pp. 399–404.

26. Suardi N. et al. Effect of visible laser light on ATP level of anaemic red blood cell, *J. Photochem. Photobiol. B Biol*, 2016, vol. 162, pp. 703–706.

10. Kujawa J. et al. Effect of Low-Intensity (3.75–25 J/cm^2) Near-Infrared (810 nm) Laser Radiation on Red Blood Cell ATPase Activities and Membrane Structure // J. Clin. Laser Med. Surg. – 2004. – Vol. 22, № 2. – P. 111–117.

11. Al Musawi M.S. et al. Erythrocyte sedimentation rate of human blood exposed to low-level laser // Lasers Med. Sci. Lasers in Medical Science. – 2016. – Vol. 31, № 6. – P. 1195–1201.

12. Mitrofanis J. et al. The potential of light therapy in Parkinson's disease // ChronoPhysiology Ther. – 2014. № February.

13. Shaw V.E. et al. Neuroprotection of midbrain dopaminergic cells in MPTP-treated mice after near-infrared light treatment // J. ComP. Neurol. – 2010. – Vol. 518, № 1. – P. 25–40.

14. Hamblin M.R. Shining light on the head: Photobiomodulation for brain disorders // BBA Clin. The Author. – 2016. – Vol. 6. – P. 113–124.

15. Lapchak P.A., Wei J., Zivin J.A. Transcranial Infrared Laser Therapy Improves Clinical Rating Scores After Embolic Strokes in Rabbits. – 2004. – P. 1985–1988.

16. Sadeh M. et al. Low-Level Laser Therapy Applied Transcranially to Rats After Induction of Stroke Significantly Reduces Long-Term. – 2006. – P. 2620–2624.

17. Jagdeo J.R. et al. Transcranial Red and Near Infrared Light Transmission in a Cadaveric Model // PLoS One. – 2012. – Vol. 7, № 10. – P. 1–10.

18. Tedford C.E. et al. Quantitative analysis of transcranial and intraparenchymal light penetration in human cadaver brain tissue // Lasers Surg. Med. – 2015. – Vol. 47, № 4. – P. 312–322.

19. Baryshnikov G., Minaev B., Ågren H. Theory and Calculation of the Phosphorescence Phenomenon // Chem. Rev. – 2017. – Vol. 117, № 9. – P. 6500–6537.

20. Mattley Y. et al. Blood characterization using UV/vis spectroscopy. – 1995. – Vol. 2388. – P. 462–470.

21. Soltani S., Ojaghi A., Robles F.E. Deep UV dispersion and absorption spectroscopy of biomolecules // Biomed. Opt. Express. – 2019. – Vol. 10, № 2. – P. 487.

22. Brown K.A. Erythrocyte metabolism and enzyme defects // Lab. Med. – 1996. – Vol. 27, № 5. – P. 329–333.

23. Lynch E.C. Peripheral Blood Smear- Edward Lynch // Clinical Methods: The History, Physical, and Laboratory Examiniations. 3rd ed. Butterworth Publishers. – 1990. – P. 732–734.

24. Paul A. et al. The bystander effect in optically trapped red blood cells due to plasmodium falciparum infection // Trans. R. Soc. TroP. Med. Hyg. – 2013. – Vol. 107, № 4. – P. 220–223.

25. Marcel B., Lawrence S. L. The Discocyte-Echinocyte Equilibrium of the Normal and Pathologic Red Cell. – 1970. – Vol. 36, № 3. – P. 399–404.

26. Suardi N. et al. Effect of visible laser light on ATP level of anaemic red blood cell // J. Photochem. Photobiol. B Biol. – 2016. – Vol. 162. – P. 703–706.

ORIGINAL ARTICLES

LASER TECHNOLOGIES IN TREATMENT OF CERVICAL INTRAEPYTELIAL NEOPLASIA (REVIEW)

Tzerkovsky D.A.[1], Dunaevskaya V.V.[2]
[1]N.N. Alexandrov National Cancer Centre of Belarus, Lesnoy, Republic of Belarus
[2]National Cancer Institute, Kiev, Ukraine

Abstract

This review article discusses the key aspects of the use of laser technologies, namely, laser vaporization (LV) and photodynamic therapy (PDT), in the treatment of patients with cervical intraepithelial neoplasia (CIN). The authors analyzed and systematized the foreign experience of these methods of treatment, their indications and contraindications, as well as the advantages over traditional approaches to the treatment of this pathology. The main advantages of the LV are the possibility of complete evaporation of the pathological focus, visual control over the depth of tissue destruction, the absence of prolonged edema and cicatricial deformities, which allows maintaining the integrity of the cervix and its reproductive function. Despite the low trauma and low frequency of adverse reactions, the data on the effectiveness of LV are quite contradictory and, according to various authors, vary from 50% to 98%. To date, there is a significant amount of accumulated experience in the use of PDT with various photosensitizing agents (5-aminolevulinic acid (5-ALA), hematoporphyrin and chlorin and their derivatives) in the treatment of patients with CIN. The main advantages of the PDT are minimal toxicity to the surrounding normal tissues due to the selective accumulation of photosensitizer in pathological tissues, a low risk of severe pain syndrome, the absence of mechanisms of primary and acquired resistance, the possibility of an outpatient treatment session, the possibility of combining with other methods of therapeutic action, the absence of limiting cumulative doses of photosensitizers and light exposure, the possibility of multiple repetitions of the session, good cosmetic results and the possibility of implementing an organ-preserving method of treatment. The obtained results indicate good tolerability of the method (no severe adverse reactions) and a fairly high efficiency of PDT: the frequency of complete regressions varies from 30% to 67% - for application forms of 5-ALA and from 90% to 98.1% - for hematoporifirin and chlorin photosensitizers. Thus, LV and PDT can be considered safe and effective treatment options for patients with CIN.

Key words: cervical intraepithelial neoplasia, laser vaporization, photodynamic therapy.

ЛАЗЕРНЫЕ ТЕХНОЛОГИИ В ЛЕЧЕНИИ ЦЕРВИКАЛЬНОЙ ИНТРАЭПИТЕЛИАЛЬНОЙ НЕОПЛАЗИИ (ОБЗОР ЛИТЕРАТУРЫ)

Д.А. Церковский[1], В.В. Дунаевская[2]
[1]Республиканский научно-практический центр онкологии и медицинской радиологии им. Н.Н. Александрова, Лесной, Республика Беларусь
[2]Национальный институт рака, Киев, Украина

Резюме

В представленной обзорной статье рассмотрены ключевые аспекты применения лазерных технологий, а именно лазерной вапоризации (ЛВ) и фотодинамической терапии (ФДТ), в лечении пациенток с цервикальными интраэпителиальными неоплазиями (CIN). Авторы проанализировали и систематизировали зарубежный опыт данных методов лечения, показания и противопоказания к их применению и преимущества по сравнению с традиционными подходами к лечению этой патологии. Основными преимуществами метода ЛВ являются возможность полного испарения патологического очага, визуальный контроль за глубиной деструкции тканей, отсутствие длительного отека и рубцовых деформаций, что позволяет сохранить целостность шейки матки и ее репродуктивную функцию. Несмотря на малую травматичность и невысокую частоту нежелательных реакций, данные литературы об эффективности ЛВ достаточно противоречивы и варьирует от 50% до 98%. В настоящее время в мире накоплен значительный опыт применения ФДТ с различными фотосенсибилизирующими агентами (5-аминолевулиновая кислота (5-АЛК), гематопорфирин, хлорин и их производные) в лечении пациенток с CIN. Основными преимуществами метода ФДТ являются минимальная токсичность для окружающих нормальных тканей в связи с избирательным накоплением фотосенсибилизатора (ФС) в патологических тканях, невысокий риск воз-

никновения выраженного болевого синдрома, отсутствие механизмов первичной и приобретенной резистентности, возможность амбулаторного проведения сеанса лечения, возможность комбинации с другими методами лечебного воздействия, отсутствие лимитирующих кумулятивных доз ФС и светового воздействия, возможность многократного повторения сеанса, хорошие косметические результаты и возможность реализации органосохраняющего метода лечения. Полученные результаты свидетельствуют о хорошей переносимости лечения и достаточно высокой эффективности применения ФДТ: частота полных регрессий варьирует от 30 до 67% при использовании аппликационных форм 5-АЛК, от 90 до 98,1% – при использовании гематопорифирина и хлориновых ФС. Таким образом, ЛВ и ФДТ могут рассматриваться как безопасные и эффективные опции лечения пациенток с CIN.

Ключевые слова: цервикальная интраэпителиальная неоплазия, лазерная вапоризация, фотодинамическая терапия.

Introduction

Cervical dysplasia or cervical intraepithelial neoplasia (CIN) is a serious disease caused by the presence of human papilloma viruses (HPV) of high oncogenic risk [1]. CIN is most commonly found in young women (25–35 y. o.). This is due to the fact that at this age, HPV elimination processes are already completed, and if they have not occurred, then the negative effect of the viruses can be activated.

There are three degrees of cervical dysplasia: light (CIN I), medium (CIN II) and severe (CIN III). All of them are links in the same chain, and it is believed that CIN I and CIN II are reversible processes, and CIN III is considered to be a precancerous disease. Due to the etiological role of HPV in cervical carcinogenesis, the initial stages of cervical cancer are regarded as HPV-associated diseases: HPV DNA is detected in 25% of cases of CIN I, in 80% of cases of CIN II, and up to 96% of cases of CIN III. The risk of malignancy is associated with the presence of several high-risk HPV genotypes: 16, 18, 31, 33, 35 and 45. It was found that the presence of oncogenic HPV genotypes serves as a prognostic factor for the development of CIN. HPV, mainly its 16 and 18 genotypes, is detected in 50–80% of spesimens of moderate and severe cervical squamous epithelium dysplasia and in 90% of cases of invasive cancer [2].

Timely diagnosis and effective treatment of CIN provide secondary prevention of cervical cancer [3]. The existing treatment methods can be divided into surgical and destructive ones. The first category includes cold-knife, laser and radio wave excision, and the second consists of laser vaporization (LV), diathermocoagulation and cryodestruction. All the listed methods of treatment have a direct impact on the pathological focus without affecting the mechanisms of disease development. However, their use may lead to the development of a number of undesirable reactions, such as pain, bleeding, lymphorrhea and tissue trauma, leading to the formation of rough scars on the cervix and the stenosis of the cervical canal, accompanied by changes in the anatomical structure of the cervix, and, as a result, to a decrease in the probability of conception, an increased risk of miscarriages, and also prevents natural delivery [3].

Laser vaporization

The use of aser technologies in the treatment of CIN plays an important role and is especially indicated for young patients with a verified diagnosis of CIN I – III, as well as when there are contraindications to the use of traditional methods of treatment or when patients refuse to use them.

One of these methods is LV, a treatment method based on the use of a focused laser beam with a diameter of up to 1 mm from a high-energy laser with a radiation power of up to 20 watts. LV is indicated for nulliparous women under the age of 40 with CIN II degree of pathological changes in the cervical epithelium. The main advantages of the method are the possibility of complete evaporation of the pathological focus, visual control of the depth of tissue destruction, and the absence of long-term edema and scar deformities, which allows for cervix integrity preservation and makes it possible to maintain its reproductive function [4].

Despite the low degree of injury and low rate of adverse reactions, the effectiveness of LV, according to various authors, varies from 50% to 98% [5,6,7,8,9].

J. A. Jordan presented the experience of treating 711 patients using the CO_2 LV method. During the follow-up period (20 months), the frequency of complete tumor regression (CTR) was 95% [5].

According to Fallani M. G. et al. (Department of Gynecology, University of Florence, Italy), the use of LV resulted in 97.5% CTR in 157 patients with CIN II – III [6]. The treatment of 94 patients with CIN III by LV, according to M. Fambini et al. (Department of Gynecology, University of Florence, Italy) resulted in CTR in 91.5% of cases. When partial regression or stabilization of the

pathological process was achieved, further treatment sessions were provided. In 32.7% of cases, an adverse reaction was noted in the form of moderate bleeding during the treatment session [7].

According to E. Saah-Briffaut (Clinique de Gyné-cologie, Hôpital Jeanne-de-Flandre, France), the use of LV in 52 patients with CIN II – III allowed to achieve CTR only in 67.3% of cases [8].

B. S. Yoon et al. (Department of Obstetrics and Gy-necology, CHA Gangnam Medical Center, South Korea) treated 141 CIN II patients with LV. The authors reported that the main factor determining the effectiveness of the method is the depth of ablation of pathological foci. The CTR rate was 90.1% [9].

At the same time, one can mention that ulceration, bleeding and secondary infection are observed among the adverse reactions that develop against the back-ground of LV treatment. Another disadvantage is the method's inability to eliminate HPV, the virus which causes the development of CIN.

Photodynamic therapy

In connection with all the above, there is a need to search for new organ-preserving methods of CIN treat-ment. One of these methods is photodynamic therapy (PDT), a method based on the use of special substances referred to as photosensitizers (PS), which selectively ac-cumulate in pathologically altered tissues. Subsequent exposure to laser radiation of a certain wavelength leads to the launch of a cascade of photochemical re-actions, which result in the formation of a significant amount of free radicals and the initiation of oxidative stress syndrome in pathological tissues, leading to their death as a result of apoptosis and/or necrosis [10, 11, 12, 13, 14, 15, 16].

Important advantages of PDT in comparison with traditional methods of CIN treatment are the selectivity of exposure, the possibility of combining therapeutic and diagnostic options, the absence of the risk of seri-ous adverse reactions which are typical for surgery, the relative cost-effectiveness of the method and the pos-sibility of its repeated use.

The choice of a sparing and organ-preserving PDT method for young women with varying CIN stages is due to the desire to provide reliable treatment of pa-tients and preserve their menstrual and reproductive functions, which is important for women planning pregnancy [17,18].

The use of PDT can not only effectively produce the desired effect on the pathological focus, but also leads to the eradication of HPV, thereby preventing a relapse. Currently, the world has accumulated considerable ex-perience in the use of PDT with various photosensitiz-ing agents (5-aminolevulinic acid (5-ALA), hematopor-phyrin, photofrin II, chloride and its derivatives) in the treatment of patients with CIN.

Photodynamic therapy with 5-aminolevulinic acid

P. Hillemanns was among the first to use PDTs with the 5-ALA in application form (Department of Obstetrics and Gynecology, Ludwig-Maximilians-University, Ger-many) in the treatment of 10 patients with CIN II – III. Ir-radiation of pathological foci was performed 3–5 hours after local application of 10 ml of 20% solution of 5-ALA, the dose of light energy is 100 J/cm^2, the radiation pow-er density is 100–150 mW/cm^2 (λ=635 nm). No serious adverse reactions were reported after the treatment. Several patients had moderate pain syndrom and vagi-nal discharge. The author reported that at the follow-up 3 months later, the frequency of CTR was 30% (n=3), and the remaining patients underwent cold-knife con-ization of the cervix due to insufficient effectiveness of the previous treatment [19].

A. Barnett et al. (School of Biomedical Sciences, Uni-versity of Leeds, UK) reported poor PDT performance using 3% 5-ALA gel (Intrasite Gel®, Smith & Nephew Healthcare Ltd., Hull, UK) in 12 patients with CIN I – II in-cluded in a double-blind placebo-controlled random-ized trial. 13 patients in the control group were treated with a gel that did not contain 5-ALA. Irradiation of pathological foci of the cervix was carried out 4 hours after local application of 3% 5-ALA gel, the dose of light energy being 100 J/cm^2, the radiation power density was 100 mW/cm^2 (λ=635 nm). There were no serious adverse reactions to the treatment, only 3 patients from the main group complained of discomfort and mod-erate pain during the PDT session. The CTR rate in the main group was 33%, whereas in the control group it was 31%. The authors did not reveal any statistically significant differences in the results of the treatment of patients in the comparison groups (p>0.05) [20].

K. A. Keefe et al. (Division of Gynecologic Oncology, Chao Family Compressive Cancer Center, USA) reported the results of phase I and II of the clinical trial of PDT tolerability and efficacy with the application form 5-ALA (200 mg/ml) in 40 patients with CIN II (n=16) and CIN III (n=24). The authors used an escalation of the light en-ergy dose from 50 to 150 J/cm^2 (λ=630 nm), irradiation was carried out 1.5 hours after the application of 5-ALA to tissues with pathological changes. No serious ad-verse reactions to the treatment were observed, howev-er, several patients mentioned discomfort and moder-ate pain during irradiation. Cytological and colposcopic control in 4 months after treatment resulted in CTR rate of 51%, in 8 months, a 46% rate, and 31% in 12 months. The authors concluded that the therapeutic effect did not depend of the light energy dose [21].

P. Soergel et al. (Department of Obstetrics and Gyne-cology, Hannover Medical School, Germany) reported on their experience of administering PDT treatment

with a gel form of hexaminolevulinate (thermogel) in 24 patients with CIN I – III. Irradiation of the cervix and cervical canal (λ=633 nm) was carried out 3–5 hours after gel application. No serious adverse events were observed after PDT. The follow-up after 6 months showed that CTR rate reached 63%. Patients had a long 6-month HPV remission: at CIN I-71%, CIN II-50% and CIN III-71% [22]. In the general group of patients (CIN I – III), the CTR rate was 67% [23].

In a literature review that included an analysis of the results of 14 clinical trials (472 patients with CIN I – III), K. N. Tao systematized the experience of using PDT with 5-ALA and porphyrinic PS agents [24]. The author reported that the CTR rate in the compared studies varied from 0 to 100%, and the effectiveness of HPV eradication was from 53.4 to 80% [25].

E. G. Novikova et al. (FSBI P. A. Hertsen MORC of the Ministry of Health of the Russian Federation) reported on the use of PDT with 20% 5-ALA ointment in 40 patients with primary cervical cancer after previous organ-preserving surgery (high cone-shaped amputation of the cervix). Irradiation was performed 6 hours after ointment application; a diode laser was used, its wavelength corresponding to 635 nm, the dose of light energy being 150 J/cm^2, and the radiation power density was 150–250 mW/cm^2. PDT of the cervical canal was performed with a flexible monofilament quartz light guide with a cylindrical diffuser providing a 360° light matrix, with the length of 1 cm corresponding to the length of the endocervix. Irradiation of the vaginal portion of the cervical stump was performed remotely via a light guide with a lens perpendicular to the organ and a spot diameter from 1.5 to 2.0 cm. No serious adverse events were observed. Complete eradication of HPV after one course of PDT of the cervical stump was achieved in 95% of cases, and in 5% of cases, after 2 courses of PDT [2].

Photodynamic therapy with the use of hematoporphyrin and its derivatives

The results of PDT with the use of ether polyaminopropyl (PHE) in the treatment of 31 patients with CIN II – III were published by H. Ichimura et al. (Department of Obstetrics and Gynecology, Hyogo Medical Center for Adults, Japan). Irradiation was performed 60 h after intravenous infusion of PS at a dose of 2 mg/kg of body weight, with a wavelength of 630 nm, a dose of light energy of 100 J/cm^2. No serious adverse events were observed. The CTR rate recorded during morphological examination 3 months after PDT was 90%, while the share of HPV-negative patients was 76%. The follow-up after 12 months showed that CTR rate reached 100% [26].

Two years later, Yamaguchi S. et al. (Departments of Gynecology and Pathology, Osaka City General Hospital, Japan) presented data on successful PDT treatment with intravenous Photofrin administered at a dose of 2 mg/kg body weight in 105 patients with CIN I – III. Irradiation, as in the previous study, was performed with a wavelength of 630 nm, and the light energy dose of 100 J/cm^2. CTR rate 3 months after the treatment was 90%. The percentage of HPV-negative patients at the follow-up at 3, 6 and 12 months after treatment was 75%, 74% and 72%, respectively. However, it is worth noting the high frequency of adverse reactions: moderate phototoxicity was recorded in 50 (48%) of 105 patients [27].

M. C. Choi et al. (Department of Obstetrics and Gynecology, Comprehensive Gynecologic Cancer Center, South Korea) investigated the effectiveness of PDT in combination with electrosurgical excision and cervical conization in 73 patients with CIN II – III [28]. Irradiation was performed 48 hours after intravenous administration of porphyrin-type PS (Photofrin) at a dose of 2 mg/kg of body weight, using a laser with a wavelength of 630 nm. The frequency of CTR during the 12-month follow-up period was 98.1%. HPV eradication was achieved in 89.8% and 87%, respectively, at the follow-up 3 months and 12 months after PDT. The frequency of adverse reactions in the form of cutaneous phototoxicity and cervical canal stenosis was 13.6%.

C. H. Jeong compared the effectiveness of PDT with intravenous Photohem administration at a dose of 2 mg/kg body weight and diathermoelectroconization in 2 groups of patients with CIN II–III. Each group included 48 patients. The CTR rate was 93% and 95%, respectively, and HPV was not detected in 84% and 82% of cases. The author came to the conclusion that PDT can be used as an alternative method for selective destruction of pathological tissues, which allows for preserving women's fertility after treatment [29].

Y. K. Park et al. (Department of Obstetrics and Gynecology, Dankook University College of Medicine, South Korea) presented the experience of PDT treatment of 19 CIN II – III patients with the use of an injectable form of Photohem (2 mg/kg body weight) and Photofrin II (2 mg/kg body weight). Irradiation was performed 48 hours after the introduction of PS at a wavelength of 630 nm and a dose of light energy of 240 J/cm^2. The adverse reactions reported by the authors included skin phototoxicity and moderate pain during the PDT session. The CTR rate was 91% [30].

Photodynamic therapy with chlorin-type photosensitizers

Belarusian researchers (the National Cancer Center of the Republic of Belarus) presented their experience of PDT with an injectable form of Photolon, a chlorine PS, in 112 patients with CIN II–III [31]. Irradiation of the cervix and cervical canal was performed with light energy doses from 100 to 150 J/cm^2 (λ=660±5 nm), 2.5–

Таблица
Опыт применения ФДТ с различными ФС в лечении пациенток с CIN
Table
Experience of using PDT with various PS in the treatment of patients with CIN

Автор, год исследования Author, year of research	Диагноз, число пациентов Diagnosis, number of patients	ФС PS	Параметры облучения Photoirradiation parameters	Частота полной регрессии (ПР) Percentage of complete regressions (CR)	Частота элими-нации ВПЧ Percentage of complete HPV eliminations
6: *5-АЛК и ее производные (аппликационная форма)* *5-ALA and its derivatives (application form)*					
Hillemanns P., 1999 [19]	CIN II-III, n=10 CIN II-III, n=10	20% раствор 5-АЛК 20% solution 5-ALA	100 Дж/см² 100–150 мВт/см² λ=635 нм 100 J/cm² 100–150 mW/см² λ=635 nm	30% 30%	
Barnett A., 2003 [20]	CIN I-II, n=25 12 – с ФДТ 13 – без ФДТ CIN I-II, n=25 12 – with PDT 13 – without PDT	3% раствор 5-АЛК (в Intrasite Gel°) 3% solution 5-ALA (in Intrasite Gel°)	100 Дж/см² 100 мВт/см² λ=635 нм 100 J/cm² 100 mW/cm² λ=635 nm	с ФДТ – 33% без ФДТ – 31% with PDT – 33% without PDT – 31%	
Keefe K.A., 2002 [21]	CIN II (n=16) CIN III (n=24) CIN II (n=16) CIN III (n=24)	20% раствор 5-АЛК 20% solution 5-ALA	50–150 Дж/см² 0,8 Вт/см² λ=630 нм 50–150 J/см² 0,8 W/cm² λ=630 nm	частота ПР: ч/з 4 мес – 51%; ч/з 8 мес – 46%; ч/з 12 мес – 31% CR rate: thr. 4 mon. – 51%; thr. 8 mon. – 46%; thr. 12 mon. – 31%;	
Soergel P., 2008 [22]	CIN I (n=7) CIN II (n=10) CIN III (n=7) CIN I (n=7) CIN II (n=10) CIN III (n=7)	гексамино-левулинат термогель 10 mM hexamino-levulinate thermogel 10 mM	λ=633 нм λ=633 nm	63% 63%	71%; 50%; 71% 71%; 50%; 71%
6: *Гематопорфирин и его производные (инъекционная форма)* *Hematoporphyrin and its derivatives (injectable form)*					
Ichimura H., 2003 [26]	CIN II (n=2) CIN III (n=29) CIN II (n=2) CIN III (n=29)	полигемато-порфирин эфир, 2 mg/kg polyhemato-porphyrin ether, 2 mg/kg	100 Дж/см² λ=630 нм 100 J/cm² λ=630 nm	ч/з 3 мес – 90%; ч/з 12 мес – 100%. thr. 3 mon. – 90%; thr. 12 mon – 100%	76% 76%
Yamaguchi S, 2005 [27]	CIN I-III, n=105 CIN I-III, n=105	фотофрин, 2 мг/кг photofrin, 2 mg/kg	100 Дж/см² λ=630 нм 100 J/cm² λ=630 nm	90%. 90%	3–12 мес – 72–75% thr.3–12 mon – 72–75%
Choi M.C., 2013 [28]	CIN II-III, n=73 CIN II-III, n=73	фотофрин, 2 мг/кг photofrin, 2 mg/kg	100 Дж/см² λ=630 нм 100 J/cm² λ=630 nm	98,1%. 98,1%	ч/з 3 мес – 89,8%; ч/з 12 мес – 87% thr. 3 mon. – 89,8%; thr. 12 mon. – 87%

Автор, год исследования Author, year of research	Диагноз, число пациентов Diagnosis, number of patients	ФС PS	Параметры облучения Photoirradiation parameters	Частота полной регрессии (ПР) Percentage of complete regressions (CR)	Частота элиминации ВПЧ Percentage of complete HPV eliminations
Jeong C.H., 2015 [29]	CIN II-III, n=48 CIN II-III, n=48	фотогем, 2 мг/кг photogem, 2 mg/kg	>200 Дж/см² λ=630 нм >200 J/cm² λ=630 nm	CIN II – 93% CIN III – 95% CIN II – 93% CIN III – 95%	CIN II – 84% CIN III – 82% CIN II – 84% CIN III – 82%
Park Y.K., 2016 [30]	CIN II-III, n=23 CIN II-III, n=23	фотогем 2 мг/кг (n=2), фотофрин, 2 мг/кг photogem 2 mg/kg (n=2), photofrin 2 mg/kg	240 Дж/см² 0,4 Вт, λ_1=632 нм, λ_2=630 нм 240 J/cm² 0,4 W, λ_1=632 nm, λ_2=630 nm	91% 91%	
Хлорин и его производные (инъекционная форма) *Chlorin and its derivatives (injectable form)*				
Istomin Yu.P., 2010 [31]	CIN II-III, n=112 CIN II-III, n=112	фотолон, 2–2,5 мг/кг photolon 2–2,5 mg/kg	100–150 Дж/см² 0,5–0,6 Вт, λ=660±5 нм 100–150 J/cm² 0,5–0,6 W, λ=660±5 nm	92,8% 92.8%	53,4% (у 47 из 88) 53.4% (47 out of 88)
Отдельнова О.Б., 2008 [33] Otdelnova O.B., 2008 [33]	фоновые и предраковые заболевания шейки матки, n=72 pre-existing and precancerous diseases of the cervix, n=72	фотодитазин (0,5% гель и/или 0,5 мг/кг) fotoditazin (0.5% gel or 0.5 mg/kg)	80–250 Дж/см², λ=662 нм 80–250 J/cm², λ=662 nm	88,9% 88.9%	
Гребенкина Е.В., 2014 [34] Grebenkina E.V., 2014 [34]	CIN III (n=8), cancer in situ (n=4) CIN III (n=8), cancer in situ (n=4)	фотолон, 0,75–1,15 мг/кг photolon, 0,75–1,15 mg/kg	150 Дж/см² 400–500 мВт/см² λ=660 нм 150 J/cm² 400–500 mW/cm² λ=660 nm	у 4 пациенток эффект оценен как ПР, у 7 обнаружена CIN I, у 1 – CIN II. in 4 patients, the effect was assessed as CR, in 7 patients CIN I was found, in 1 – CIN II.	80% 80%
Филоненко Е.В., 2015 [35] Filonenko E.V., 2015 [35]	CIN II (n=5) CIN III (n=13) CIN II (n=5) CIN III (n=13)	радахлорин, 1 мг/кг radachlorin, 1 mg/kg	300–350 Дж/см², λ=662 нм 300–350 J/cm², λ=662 nm	CIN II – 100% CIN III – 77% CIN II -100% CIN III – 77%	
Никонов С.Д., 2019 [36] Nikonov S.D., 2019 [36]	CIN III, cancer in situ n=43 CIN III, cancer in situ n=43	фотодитазин, радахлорин, 1 мг/кг fotoditazin, radachlorin, 1 mg/kg	0,4 Вт, λ=662 нм 0,4 W, λ=662 nm	95,35% 95.35%	

3.0 hours after the end of the PS infusion. At the first stage, the vaginal part of the cervix was remotely irradiated with a fiber-optic light guide with a microlens. When the size of the CIN focus did not exceed 3 cm, irradiation was performed with a single field with a diameter of 4 cm. If the size of the pathological focus exceeded 3 cm, 4 fields with a diameter of 2.0 to 2.5 cm were irradiated. At the second stage, the entire length of the cervical canal was irradiated with a fiber-optic catheter which had a cylindrical diffuser. There were no serious adverse reactions to the treatment; however, several patients showed discomfort, moderate pain during irradiation, and vaginal discharge. According to the authors, the CTR rate detected 3 months after treatment was 92.8%, and complete HPV eradication was observed in 53.4% of cases.

In a later study, the authors summarized the experience of PDT use in patients with CIN II (n=230) and CIN III (n=378) treated between 2006 and 2019. Follow-up observations for a period of 3 months or more found only occasional cases of cervical canal stenosis and coagulated cervix syndrome. The CTR rate determined in 2.5–3.0 months after PDT in the group of patients with CIN II reached 100%, with CIN III, 94.1% [32].

O.B. Otdelnova et al. (N.I. Pirogov Russian State Medical University, Department of Obstetrics and Gynecology, Russian Federation) presented the results of PDT treatment of 72 patients with background and precancerous diseases of the cervix. The photosensitizing agent was Photoditazine, in application (0.5% gel) and injection (0.5 mg/kg body weight) forms. Irradiation of the cervix and cervical canal was performed 1.5–2.0 hours after the introduction of PS (λ=662 nm). Depending on the nature of the pathological process, the duration of exposure varied from 15 to 40 minutes, and the dose of light energy from 80 to 250 J/cm^2. The control group used for comparison was administered diathermosurgical treatment (diathermocoagulation and diathermoconization) with the ES 500 M device (Russia). There were no serious adverse reactions after PDT, and side effects in the form of incomplete cervical epithelization were observed in 8 (11.1%) patients. In the control group, 76.6% of patients suffered from pain in the lower abdomen, 6.7% of patients had bleeding in the postoperative period, 6.7% had exacerbation of chronic salpingoophoritis, 30% had colpitis, 20% had incomplete epithelialization of the cervix. With the use of PDT, the CTR rate was 88.9%, which was confirmed by the results of colposcopy and cytological tests [33].

E.V. Grebenkina et al. (Nizhny Novgorod Regional Cancer Dispensary, Russian Federation) presented the results of PDT in 8 patients with CIN III and 4 patients with cancer in situ. Photolon was administered intravenously at a dose of 0.75–1.15 mg/kg of body weight. After 1.5–2.0 hours, an irradiation session was performed with a light energy dose of 150 J/cm^2. Laser radiation was delivered to the endocervix with quartz light guides with 3 cm long cylindrical diffusers providing a 360° light matrix, and a macro lens with a light spot from 1 to 2 cm in diameter was applied to the vaginal portion of the cervix. 30 days after treatment, cervical conization was performed with cervical canal curettage, and the results of PDT were evaluated. During PDT, no serious adverse reactions were registered, the irradiation session was well tolerated, and only 2 patients had pain syndrome (pain in the lower abdomen) during the PDT session. According to the histological study of postoperative material, the effect of treatment in 4 patients was estimated as CTR, CIN I was detected in 7 patients, and CIN II in one. HPV eradication was achieved in 80% of cases [34].

E.V. Filonenko et al. published the results of phase III clinical trials of Radachlorin use in PDT in 30 patients with precancerous diseases and initial cervical cancer: ectopia – 4 cases, CIN II – 5 cases, CIN III – 13 cases, carcinoma in situ – 4 cases, stage Ia of cervical cancer – 4 cases. PS was administered once, intravenously at a dose of 1 mg per kilo of body weight 3 hours before irradiation, and light energy doses from 300 to 350 J/cm^2 (λ = 662 nm) were used. The PDT session of the cervical canal was performed via a quartz light guide with a cylindrical diffuser from 1 to 3 cm long along the entire length of the cervical canal, and the vaginal part of the cervix was irradiated via a macro lens with a light spot diameter from 2 to 3 cm, depending on the anatomical characteristics of the organ. No serious adverse events were observed after PDT. The CTR rate in patients with CIN II and III was 100% and 77%, respectively [35].

S.D. Nikonov et al. (FBHI "Primorsky Regional Cancer Dispensary", Russian Federation) in their study evaluated the effectiveness of PDT HPV-associated CIN III and carcinoma in situ in 43 nulliparous patients who refused to undergo conization. Injectable forms of photoditazine (1 mg/kg body weight) and radachlorine (1 mg/kg body weight) with an exposure of 3 hours were used as PS. Irradiation was performed with Lakhta-Milon and Latus lasers (λ=662 nm). Exocervix PDT was performed remotely, monopositionally, via a light guide with a collimator at a radiation power of 2 W and a light spot diameter of 4 cm. PDT of the cervical canal was performed via a light guide with a cylindrical diffuser 4 cm long with a radiation power of 0.4 W. Complete recovery was observed in 95.35% of cases, and in the subgroup of nulliparous patients, in 96.3% (n=26), which was confirmed by the elimination of all types and combinations of HPV, as well as a successful colposcopic and cytological picture [36].

To summarize the above data on the effectiveness of PDT in various research centers and clinics in the CIS, Europe, Southeast Asia, and the United States, the data

on the effectiveness of PDT in various studies are summarized in the table.

Conclusion

Thus, the effectiveness of PDT in the treatment of patients with CIN depends on the PS chemical structure and the method of its administration. In most cases, the highest efficiency is achieved with systemic (intravenous) administration of PS [2, 21, 22, 23, 24, 25, 26, 27, 28, 29, 30], while the use of 5-ALA application forms (solutions, gels and ointments) does not lead to a high CTR rate [14, 15, 16, 17, 18]. The above results of studies conducted by various authors confirm the ample opportunities of PDT use in the treatment of patients with CIN, which is possible due to the fact that this method has a number of advantages compared to the existing standard methods of treatment.

The main advantages of PDT include:
- minimal toxicity to surrounding normal tissues, due to selective accumulation of PS in pathological tissues;
- low risk of severe pain syndrome;
- negligible system effects;
- lack of primary and acquired resistance mechanisms;
- possibility of administering treatment sessions on outpatient basis;
- possibility of combination with other treatment methods;
- the absence of limiting cumulative doses of PS and light exposure, the possibility to repeat the treatment;
- good cosmetic results;
- organ-sparing approach.

REFERENCES

1. Santesso N., Mustafa R.A., Wiercioch W. et al. Systematic reviews and meta-analyses of benefits and harms of cryotherapy, LEEP, and cold knife conization to treat cervical intraepithelial neoplasia, *Int. J. Gynecol. Obst*, 2016, vol. 132, pp. 266–271.
2. Novikova E.G., Trushina O.I. Photodynamic therapy in the prevention of human papillomavirus (HPV) - associated recurrence of cervical cancer, *Oncogynecology*, 2015, No. 2, pp. 25–31. (in Russ.)
3. Laptsevich T.P., Istomin Yu.P., Chalov V.N. Photodynamic therapy with a photolon of cervical intraepithelial neoplasia II-III degree, *Laser medicine*, 2009, vol. 13(3), pp. 30–35. (in Russ.)
4. Laptsevich T.P., Istomin Yu.P., Chalov V.N. Photodynamic therapy of cervical intraepithelial neoplasia, *LAP LAMBERT Academic Publishing GmbH,* 2011, p. 109. (in Russ.)
5. Jordan J.A., Woodman C.B., Mylotte M.J. et al. The treatment of cervical intraepithelial neoplasia by laser vaporization, *Br. J. Obstet. Gynaecol,* 1985, vol. 92(4), pp. 394–398.
6. Fallani M.G. Laser CO2 vaporization for high-grade intraepithelial neoplasia: a long-term follow-up series, *Gynecol. Oncol*, 2003, vol. 91(1), pp. 130–133.
7. Fambrini M., Penna C., Pieralli A. et al. CO2 laser cylindrical excision or standard re-conization for persistent-recurrent high-grade cervical intraepithelial neoplasia (HG-CIN) in women of fertile age, *Anticancer Res*, 2008, vol. 28(6), pp. 3871–3875.
8. Saah-Briffaut E., Collinet P., Saah R. et al. Treatment of squamous intraepithelial lesion of type CIN2 et CIN3 with laser CO2 vaporization: retrospective study of 52 cases, *J. Gynecol. Obstet. Biol. Reprod (Paris)*, 2006, vol. 35(8), pp. 785–789.
9. Yoon B.S., Seong S.J., Song T. et al. Risk factors for treatment failure of CO2 laser vaporization in cervical intraepithelial neoplasia 2, *Arch. Gynecol. Obst*, 2014, vol. 290(1), pp. 115–119.
10. Abdel-Kader M.H. Photodynamic therapy. From theory to application, *Verlag, Berlin, Heidelberg* : Springer, 2014, p. 312.
11. Dougherty T.J., Gomer C.J., Henderson B.W. Photodynamic therapy, *J. Natl. Cancer Inst*, 1998, vol. 90(12), pp. 889–905.
12. Agostinis P., Berg K., Cengel K.A. Photodynamic therapy of cancer: an update. *CA: A Cancer J. Clin*, 2011, vol. 61, pp. 250–281.
13. Sokolov, V.V., Chissov, V.I., Filonenko, E.V. et al. Photodynamic therapy of cancer with the photosensitizer PHOTOGEM, *Proceedings of SPIE - The International Society for Optical Engineering*, 1995, vol. 2325, pp. 367–374.

ЛИТЕРАТУРА

1. Santesso N., Mustafa R.A., Wiercioch W. et al. Systematic reviews and meta-analyses of benefits and harms of cryotherapy, LEEP, and cold knife conization to treat cervical intraepithelial neoplasia. // Int. J. Gynecol. Obst. – 2016. – Vol. 132. – P. 266–271.
2. Новикова Е.Г., Трушина О.И. Фотодинамическая терапия в профилактике ВПЧ-ассоциированных рецидивов рака шейки матки // Онкогинекология. – 2015. – № 2. – С. 25–31.
3. Лапцевич Т.П., Истомин Ю.П., Чалов В.Н. Фотодинамическая терапия с фотолоном цервикальной интраэпителиальной неоплазии II-III степени // Лазерная медицина. – 2009. – Т. 13, вып. 3. – С. 30–35.
4. Лапцевич Т.П., Истомин Ю.П., Чалов В.Н. Фотодинамическая терапия цервикальной интраэпителиальной неоплазии // LAP LAMBERT Academic Publishing GmbH. – 2011. – p .109.
5. Jordan J.A., Woodman C.B., Mylotte M.J. et al. The treatment of cervical intraepithelial neoplasia by laser vaporization // Br. J. Obstet. Gynaecol. – 1985. – Vol. 92(4). – P. 394–398.
6. Fallani M.G. Laser CO$_2$ vaporization for high-grade intraepithelial neoplasia: a long-term follow-up series // Gynecol. Oncol. – 2003. – Vol. 91(1). – P. 130–133.
7. Fambrini M., Penna C., Pieralli A. et al. CO$_2$ laser cylindrical excision or standard re-conization for persistent-recurrent high-grade cervical intraepithelial neoplasia (HG-CIN) in women of fertile age // Anticancer Res. – 2008. – Vol. 28(6). – P. 3871–3875.
8. Saah-Briffaut E., Collinet P., Saah R. et al. Treatment of squamous intraepithelial lesion of type CIN2 et CIN3 with laser CO2 vaporization: retrospective study of 52 cases // J. Gynecol. Obstet. Biol. Reprod (Paris). – 2006. – Vol. 35(8). – P. 785–789.
9. Yoon B.S., Seong S.J., Song T. et al. Risk factors for treatment failure of CO$_2$ laser vaporization in cervical intraepithelial neoplasia 2 // Arch. Gynecol. Obst. – 2014. – Vol. 290(1). – P. 115–119.
10. Abdel-Kader M.H. Photodynamic therapy. From theory to application // Verlag, Berlin, Heidelberg : Springer, 2014. – P. 312.
11. Dougherty T.J., Gomer C.J., Henderson B.W. Photodynamic therapy // J. Natl. Cancer Inst. – 1998. – Vol. 90(12). – P. 889–905.
12. Agostinis P., Berg K., Cengel K.A. Photodynamic therapy of cancer: an update // CA: A Cancer J. Clin. – 2011. – Vol. 61. – P. 250–281.
13. Sokolov, V.V., Chissov, V.I., Filonenko, E.V. et al. Photodynamic therapy of cancer with the photosensitizer PHOTOGEM // Proceedings of SPIE - The International Society for Optical Engineering. – 1995. – Vol. 2325. – P. 367–374.

14. Filonenko, E.V. The history of development of fluorescence diagnosis and photodynamic therapy and their capabilities in oncology, *Russian Journal of General Chemistry*, 2015, vol. 85(1), pp. 211–216.

15. Yakubovskaya, R.I., Morozova N.B., Pankratov A.A., et al. Experimental photodynamic therapy: 15 years of development, *Russian Journal of General Chemistry*, 2015, vol. 85(1), pp. 217 – 239.

16. Petrishchev N.N., Galkin M.A., Grishacheva T.G., et al. The effect of chlorin e6 drug on platelet aggregation activity, *Biomedical Photonics*, 2019, vol. 8(3), pp. 4–10. (In Russ.) https://doi.org/10.24931/2413–9432–2019–8-3–4-10

17. Laptsevich T.P., Istomin Yu.P., Chalov V.N. Methods of treatment of cervical intraepithelial neoplasias: reality and prospects, *Medical news*, 2008, No.9, pp. 10–16. (in Russ.)

18. Larkin A.I., Trukhanov K.A. Operational analysis of complex medical states by photonics methods, *Biomedical Photonics,* 2018, vol. 7(1), pp. 28–31. (In Russ.) https://doi.org/10.24931/2413–9432–2018–7-1–28–31

19. Hillemanns P, Korell M, Schmitt-Sody M, Baumgartner R. et al. Photodynamic therapy in women with cervical intraepithelial neoplasia using topically applied 5-aminolevulinic acid, *Int. J. Cancer*, 1999, vol. 81(1), pp. 34–38.

20. Barnett A.A., Haller J.C., Cairnduff F. et al. A randomised, double-blind, placebo-controlled trial of photodynamic therapy using 5-aminolaevulinic acid for the treatment of cervical intraepithelial neoplasia, *Int. J. Cancer*, 2003, vol. 103(6), pp. 829–832.

21. Keefe K.A., Tadir Y., Tromberg B. et al. Photodynamic therapy of high-grade cervical intraepithelial neoplasia with 5-aminolevulinic acid, *Lasers Surg. Med*, 2002, vol. 31(4), pp. 289–293.

22. Soergel P., Wang X., Stepp H. et al. Photodynamic therapy of cervical intraepithelial neoplasia with hexaminolevulinate, *Lasers Surg. Med*, 2008, vol. 40(9), pp. 611–615.

23. Soergel P., Dahl G.P., Onsrud M. et al. Photodynamic therapy of cervical intraepithelial neoplasia 1–3 and human papilloma virus (HPV) infection with methylaminolevulinate and hexaminolevulinate – A double-blind, dose-finding study, *Lasers Surg. Med*, 2012, vol. 44(6), pp. 468–474.

24. Yakubovskaya R.I., Pankratov A.A., Filonenko E.V. et al. Comparative experimental study of 5-ALA and 5-ALA hexyl ester specific activity, *Biomedical Photonics*, 2018, vol. 7(3), pp. 43–46. (In Russ.) https://doi.org/10.24931/2413–9432–2018–7-3–43–46

25. Tao X.H., Guan Y., Shao D. et al. Efficacy and safety of photodynamic therapy for cervical intraepithelial neoplasia: a systemic review, *Photodiagnosis Photodyn. Ther*, 2014, vol. 11(2), pp. 104–112.

26. Ichimura H., Yamaguchi S., Kojima A. et al. Eradication and reinfection of human papillomavirus after photodynamic therapy for cervical intraepithelial neoplasia, *Int. J. Clin. Oncol*, 2003, vol. 8(5), pp. 322–325.

27. Yamaguchi S., Tsuda H., Takemori M. et al. Photodynamic therapy for cervical intraepithelial neoplasia, *Oncology*, 2005, vol. 69, pp. 110–116.

28. Choi M.C., Jung S.J., Park H. et al. Photodynamic therapy for management of cervical intraepithelial neoplasia II and III in young patients and obstetric outcomes, *Lasers Surg. Med*, 2013, vol. 45(9), pp. 564–572.

29. Jeong C.H. 10th World Congress of the International Photodynamic Association, *Munich, Germany*, 2005, p.14.

30. Park Y.K., Park C.H. Clinical efficacy of photodynamic therapy, *Obstet. Gynecol. Sci*, 2016, vol. 59(6), pp. 479–488.

31. Istomin Yu.P., Lapzevich T.P., Chalau V.N. et al. Photodynamic therapy of cervical intraepithelial neoplasia grades II and III with Photolon, *Photodiagnosis Photodyn. Ther*, 2010, vol. 7(3), pp. 144–151.

32. Tserkovskiy D.A., Artemieva T.P. Photodynamic therapy of cervical intraepithelial neoplasia, *Evrazijskij onkologicheskij zhurnal*, 2020, vol. 8, No. 2 (Appendix), p. 355. (in Russ.)

14. Filonenko, E.V. The history of development of fluorescence diagnosis and photodynamic therapy and their capabilities in oncology // Russian Journal of General Chemistry. – 2015. – Vol. 85(1). – P. 211 – 216.

15. Yakubovskaya, R.I., Morozova N.B., Pankratov A.A. et al. Experimental photodynamic therapy: 15 years of development // Russian Journal of General Chemistry. – 2015. – Vol. 85(1). – P. 217 – 239.

16. Петрищев Н.Н., Галкин М.А., Гришачева Т.Г., Дементьева И.Н., Чефу С.Г. Влияние препарата на основе хлорина е6 на агрегационную активность тромбоцитов // Biomedical Photonics. – 2019. – Т.8, №3. – С. 4–10. https://doi.org/10.24931/2413–9432–2019–8-3–4-10

17. Лапцевич Т.П., Истомин Ю.П., Чалов В.Н. Методы лечения цервикальных интраэпителиальных неоплазий: реальность и перспективы // Медицинские новости. – 2008. – № 9. – С. 10–16.

18. Ларкин А.И., Труханов К.А. Оперативный анализ сложных медицинских состояний методами фотоники // Biomedical Photonics. – 2018. – Т.7, №1. – С.28–31. https://doi.org/10.24931/2413–9432–2018–7-1–28–31

19. Hillemanns P, Korell M, Schmitt-Sody M, Baumgartner R. et al. Photodynamic therapy in women with cervical intraepithelial neoplasia using topically applied 5-aminolevulinic acid // Int. J. Cancer. – 1999. – Vol. 81(1). – P. 34–38.

20. Barnett A.A., Haller J.C., Cairnduff F. et al. A randomised, double-blind, placebo-controlled trial of photodynamic therapy using 5-aminolaevulinic acid for the treatment of cervical intraepithelial neoplasia // Int. J. Cancer. – 2003. – Vol. 103(6). – P. 829–832.

21. Keefe K.A., Tadir Y., Tromberg B. et al. Photodynamic therapy of high-grade cervical intraepithelial neoplasia with 5-aminolevulinic acid // Lasers Surg. Med. – 2002. – Vol. 31(4). – P. 289–293.

22. Soergel P., Wang X., Stepp H. et al. Photodynamic therapy of cervical intraepithelial neoplasia with hexaminolevulinate // Lasers Surg. Med. – 2008. – Vol. 40(9). – P. 611–615.

23. Soergel P., Dahl G.P., Onsrud M. et al. Photodynamic therapy of cervical intraepithelial neoplasia 1–3 and human papilloma virus (HPV) infection with methylaminolevulinate and hexaminolevulinate – A double-blind, dose-finding study // Lasers Surg. Med. – 2012. – Vol. 44(6). – P. 468–474.

24. Якубовская Р.И., Панкратов А.А., Филоненко Е.В., Лукьянец Е.А., Иванова-Радкевич В.И., Трушин А.А., Каприн А.Д. Сравнительное экспериментальное исследование специфической активности 5-АЛК и гексилового эфира 5-АЛК // Biomedical Photonics. – 2018. – Т.7, № 3. – С. 43–46.

25. Tao X.H., Guan Y., Shao D. et al. Efficacy and safety of photodynamic therapy for cervical intraepithelial neoplasia: a systemic review // Photodiagnosis Photodyn. Ther. – 2014. – Vol. 11(2). – P. 104–112.

26. Ichimura H., Yamaguchi S., Kojima A. et al. Eradication and reinfection of human papillomavirus after photodynamic therapy for cervical intraepithelial neoplasia // Int. J. Clin. Oncol. – 2003. – Vol. 8(5). – P. 322–325.

27. Yamaguchi S., Tsuda H., Takemori M. et al. Photodynamic therapy for cervical intraepithelial neoplasia // Oncology. – 2005. – Vol. 69. – P. 110–116.

28. Choi M.C., Jung S.J., Park H. et al. Photodynamic therapy for management of cervical intraepithelial neoplasia II and III in young patients and obstetric outcomes // Lasers Surg. Med. – 2013. – Vol. 45(9). – P. 564–572.

29. Jeong C.H. 10th World Congress of the International Photodynamic Association // Munich, Germany. – 2005. – P.14.

30. Park Y.K., Park C.H. Clinical efficacy of photodynamic therapy // Obstet. Gynecol. Sci. – 2016. – Vol. 59(6). – P. 479–488.

31. Istomin Yu.P., Lapzevich T.P., Chalau V.N. et al. Photodynamic therapy of cervical intraepithelial neoplasia grades II and III with Photolon* // Photodiagnosis Photodyn. Ther. – 2010. – Vol. 7(3). – P. 144–151.

33. Otdelnova O.B., Khashukoeva A.Z., Ibragimova M.I. Possibilities of photodynamic therapy using Fotoditazin photosensitizer in the treatment of gynecological diseases, *Ross. bioter. zhurnal*, 2008, vol. 7 (4), pp. 47–52. (in Russ.)

34. Grebenkina E.V., Gamayunov S.V., Kuznetsov S.S. et al. Photodynamic therapy of diseases of the cervix, *Fotodinamicheskaya terapiya i fotodiagnostika*, 2014, No.2, pp. 12–14. (in Russ.)

35. Filonenko E.V., Serova L.G., Ivanova-Radkevich V.I. Results from phase III clinical trials with radachlorine for photodynamic therapy of pre-cancer and early cancer of cervix, *Biomedical Photonics,* 2015, vol.4 (3), pp.36–42. (In Russ.) https://doi.org/10.24931/2413–9432–2015–4-3–36–42

36. Nikonov S.D., Pasman M.N., Korotin D.A. PDT of HPV-associated cervical intraepithelial neoplasia of the third degree (CIN III) - an alternative to the refusal of nulliparous women from cervical conization, *Lazernaya meditsina*, 2019, vol. 23 (3), p. 39. (in Russ.)

32. Церковский Д.А., Артемьева Т.П. Фотодинамическая терапия цервикальной интраэпителиальной неоплазии // Евразийский онкологический журнал. – 2020. – Т. 8, № 2 (Приложение). – С. 355.

33. Отдельнова О.Б., Хашукоева А.З., Ибрагимова М.И. Возможности фотодинамической терапии с использованием фотосенсибилизатора фотодитазин в лечении гинекологических заболеваний // Росс. биотер. журнал. – 2008. – Т. 7, № 4. – С. 47–52.

34. Гребенкина Е.В., Гамаюнов С.В., Кузнецов С.С. и др. Фотодинамическая терапия заболеваний шейки матки // Фотодинамическая терапия и фотодиагностика. – 2014. – № 2. – С. 12–14.

35. Филоненко Е.В., Серова Л.Г., Иванова-Радкевич В.И. Результаты III фазы клинических исследований препарата радахлорин для фотодинамической терапии предрака и начального рака шейки матки // Biomedical Photonics. – 2015. – Т. 4, № 3. – С. 36–42.

36. Никонов С.Д., Пасман М.Н., Коротин Д.А. ФДТ ВПЧ-ассоциированной цервикальной интраэпителиальной неоплазии III степени (CIN III) – альтернатива при отказе нерожавших женщин от конизации шейки матки // Лазерная медицина. – 2019. – Т. 23, № 3. – С. 39.

REVIEWS OF LITERATURE